A Modeling Case Study of Heavy Rainstorms along the Mei-Yu Front

SHOU-JUN CHEN,* YING-HWA KUO, WEI WANG, ZU-YU TAO,* AND BO CUI+

National Center for Atmospheric Research,# Boulder, Colorado

(Manuscript received 20 November 1996, in final form 1 December 1997)

ABSTRACT

On 12–13 June 1991, a series of convective rainstorms (defined as mesoscale precipitation systems with rainfall rates exceeding 10 mm h^{-1}) developed successively along the Mei-Yu front. During this event, new rainstorms formed to the east of preceding storms at an interval of approximately 300–400 km. The successive development and eastward propagation of these rainstorms produced heavy rainfall over the Jiang-Huai Basin in eastern China, with a maximum 24-h accumulation of 234 mm. This study presents the results of a numerical simulation of this heavy rainfall event using the Penn State–NCAR Mesoscale Model Version 5 (MM5) with a horizontal resolution of 54 km.

Despite the relatively coarse horizontal resolution, the MM5, using a moist physics package comprising an explicit scheme and the Grell cumulus parameterization, simulated the successive development of the rainstorms. The simulated rainstorms compared favorably with the observed systems in terms of size and intensity. An additional sensitivity experiment showed that latent heat release is crucial for the development of the rainstorms, the mesoscale low-level jet, the mesolow, the rapid spinup of vorticity, and the Mei-Yu frontogenesis. Without latent heat release, the maximum vertical motion associated with the rainstorm is reduced from 70 to 6 cm s^{-1}.

Additional model sensitivity experiments using the Kain–Fritsch cumulus parameterization with grid sizes of 54 and 18 km produced results very similar to the 54-km control experiment with the Grell scheme. This suggests that the simulation of Mei-Yu rainstorms, the mesoscale low-level jet, and the mesolow is not highly sensitive to convective parameterization and grid resolution. In all the full-physics experiments, the model rainfall was dominated by the resolvable-scale precipitation. This is attributed to the high relative humidity and low convective available potential energy environment in the vicinity of the Mei-Yu front.

The modeling results suggest that there is strong interaction and positive feedback between the convective rainstorms embedded within the Mei-Yu front and the Mei-Yu front itself. The front provides a favorable environment for such rainstorms to develop, and the rainstorms intensify the Mei-Yu front.

1. Introduction

The rainy season (May–July) in east Asia is referred to as Mei-Yu in China and Baiu in Japan. During this period, the plum (Mei in Chinese) is ripe in the Jiang-Huai Basin, eastern China, and the rain (Yu in Chinese) occurs. In this season, a quasi-stationary front, known as the Mei-Yu front, is formed and extends from eastern China to southern Japan. The Mei-Yu front is one of the most significant circulation systems for the hydrological cycle in the east Asia monsoon region.

The synoptic structure of the Mei-Yu front is different from that of typical midlatitude fronts. The former is characterized by a weak temperature gradient, but is accompanied by a strong moisture contrast and high equivalent potential temperature (θ_e) gradient (Ding 1992). In the lower troposphere (850–700 hPa) the signatures of the Mei-Yu front in the wind field are more pronounced than in the thermal field. The front is very shallow and slopes rapidly with height. A low-level cyclonic wind shear line is located about 200–300 km north of the surface front. A well-defined synoptic-scale low-level jet (LLJ) occurs on the southern side of the shear line. It has been suggested that the LLJ transports warm, moist air northward in the lower levels; creates a convectively unstable layer (Chen 1983); and induces a secondary circulation with ascent at the northern tip of the LLJ (Chen 1982), which is favorable for the development of heavy precipitation. Reviews of the synoptic-dynamic studies on the LLJ over China and Japan can be found in Ding (1992) and Ninomiya and Murakami (1987).

Very intense and concentrated rainfall events, known

* Permanent affiliation: State Key Laboratory for Severe Storm Research, Department of Geophysics, Peking University, Beijing, China.

+ Permanent affiliation: Chinese Meteorological Center, Beijing, China.

The National Center for Atmospheric Research is sponsored by the National Science Foundation.

Corresponding author address: Dr. Ying-Hwa Kuo, NCAR/MMM Division, P.O. Box 3000, Boulder, CO 80307-3000.

as rainstorms[1] in the Mei-Yu season, are often associated with organized mesoscale disturbances and convective cloud clusters, which are embedded within and propagate along the Mei-Yu front (Fang 1985). In a case of severe flooding over Jiang-Huai Basin from 12 to 16 June 1991, Feng et al. (1995) identified 13 meso-α-scale cloud clusters and rainstorms along a Mei-Yu front based on satellite cloud-top infrared (IR) blackbody temperature (T_{bb}) and rain gauge networks. These mesoscale cloud systems and rainstorms, ranging from 100 to 500 km in size, contributed up to 415 mm of precipitation in this period. A new cloud cluster formed to the east of an old cloud cluster, like gravity waves propagating down stream. These mesoscale rainstorms cannot be resolved by the standard rawinsonde network.

Ninomiya et al. (1984) conducted a modeling study of an intensive mesoscale rainstorm along the Baiu front using a 42-km hydrostatic primitive equation numerical model. The model was able to predict both the development of a meso-α-scale depression and the concentration of rainfall, although they were considerably weaker than the analyses. The same case was studied by Nagata and Ogura (1991, hereafter referred to as NO91). Their model captured the formation of a localized surface warm front, an LLJ, and a meso-α-scale low, which were associated with the heavy precipitation. The role of diabatic heating processes in the development of the LLJ was emphasized. A numerical case study of a mesoscale convective system (MCS) that developed along a Mei-Yu front over the Taiwan area was carried out by Chen et al. (1997). They also found that the development of LLJ was sensitive to convective processes.

Since the routine radiosonde data do not have sufficient spatial and temporal resolution to resolve mesoscale rainstorms, it would be desirable to simulate rainstorms along the Mei-Yu front using a mesoscale numerical model. The dynamically consistent model output from a successful simulation, at a much higher spatial and temporal resolution, will allow a more detailed and quantitative study of the structure and evolution of rainstorms, compensating for the shortage of observational data.

This paper presents a modeling study of a heavy rainfall event that occurred on 12–13 June 1991. Dong (1991) presented a brief synoptic description of this case. The rainfall area during a 24-h period ending at 0000 UTC 13 June was oriented east–west along the Jiang-Huai Basin (Fig. 1a). Two stations recorded rainfall of over 200 mm in less than 24 h, and one station recorded 175 mm. Most of the rainfall was concentrated in the second 12-h period (1200 UTC 12 June to 0000 UTC 13 June), whereas a maximum of 72.5 mm of rain was observed between 1200 to 1800 UTC 12 June (Fig. 1e). This heavy precipitation episode was the third most severe flooding event in this area since 1950.

The objectives of this modeling study are 1) to test the ability of the Pennsylvania State University–NCAR Mesoscale Model Version 5 (MM5), with a horizontal resolution comparable to most operational models, to simulate the convective rainstorms along the Mei-Yu front; 2) to examine the mesoscale wind, temperature, and pressure structures of the rainstorms as simulated in the model; and 3) to study the governing dynamics of the rainstorms and their relationships with the Mei-Yu front. Section 2 gives a description of the MM5 model used in this study. Section 3 describes the synoptic situation. An overview of the model results is presented in section 4. The mesoscale structure of the rainstorm, LLJ, and meso-α-scale low, as simulated in the model, is analyzed in section 5 and a summary is given in section 6.

2. The mesoscale model

The MM5 is used in this study. The MM5 is a nonhydrostatic, primitive equation model with a terrain-following vertical coordinate. A total of four experiments were conducted on this case. The precipitation physics used in the control experiment (CNTL) include the mixed-phase microphysics scheme of Reisner et al. (1998), in which five prognostic equations are used for water vapor, cloud water, rainwater, cloud ice, and snow for the resolvable-scale motion, and the Grell cumulus parameterization scheme (Grell et al. 1994) for subgrid-scale convection. Blackadar's high-resolution planetary boundary layer (PBL) scheme (Zhang and Anthes 1982) is used to calculate the vertical fluxes of sensible heat, latent heat, and momentum and turbulent mixing in the PBL. A detailed description of MM5 can be found in Dudhia (1993) and Grell et al. (1994).

Figure 2a shows the model domains. These consist of an 18-km grid (D03, mesh size of 97 $\times$ 100), a 54-km grid (D02, mesh size of 79 $\times$ 85), and a 162-km grid (D01, mesh size of 62 $\times$ 82). All the grids have 23 levels in the vertical. For the CNTL experiment, only 54- and 162-km grids are activated (two-way interaction). The presentation of the CNTL will focus on the results of the 54-km grid. The locations of the relevant geographical locations referred to in the text are shown in the Fig. 2b.

The model initial conditions were obtained by objectively analyzing the radiosonde and surface observations using a successive correction scheme. The National Centers for Environmental Prediction global analyses with 2.5° resolution was used as a first guess. The operational radiosonde network in China has an average station separation of about 300 km (stations within domain D03 are plotted in Fig. 2b), which should allow

[1] There is no generally accepted definition of a rainstorm. A storm in which the local rainfall rate reaches 50 mm within 6 h is called a rainstorm in China. Here we arbitrarily define a rainstorm as a precipitation system in which the hourly rainfall rate is greater than 10 mm, reasonable for most heavy rainfall events in the Mei-Yu season.

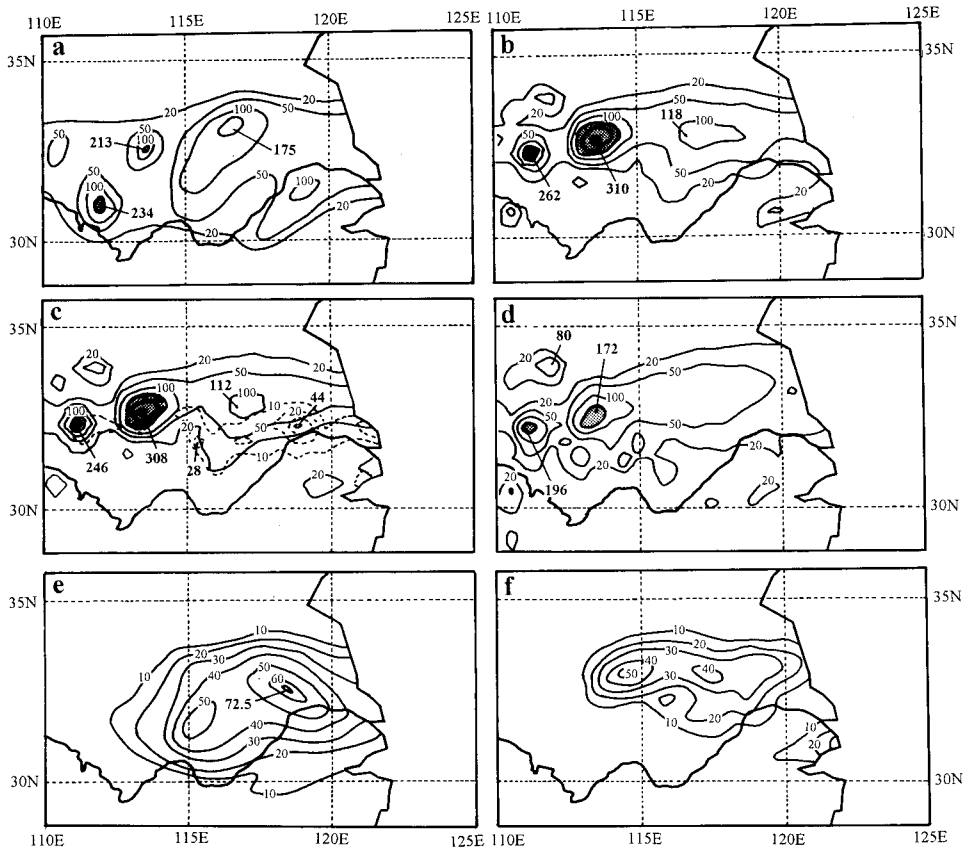

FIG. 1. (a) Observed 24-h rainfall from 0000 UTC 12 June to 0000 UTC 13 June 1991. (b) Same as (a) but for the 24 h simulated in the CNTL experiment. (c) The 24-h rainfall produced by cumulus (dashed) and explicit schemes (solid) in the CNTL experiment. (d) The 24-h rainfall produced in the KF experiment. (e) Observed 6-h rainfall from 1200 UTC to 1800 UTC 12 June 1991. (f) Same as (e) but for the 6 h simulated in the CNTL experiment. Rainfall contours are in mm. Areas of rainfall exceeding 100 mm are shaded.

the model initial condition to resolve some meso-α-scale features.[2] In this case, most of the precipitation occurred in the second 12-h period. Therefore it is a challenge to the MM5 to simulate the evolution of the rainstorms and the heavy precipitation based only on the conventional data. Previous numerical studies have shown that mesoscale features can develop in a mesoscale model initialized with the routine observations (e.g., Anthes et al. 1982; Zhang et al. 1989).

The second experiment is a ''fake-dry'' experiment (FDR), in which latent heat of condensation from both the resolvable-scale and subgrid-scale precipitation parameterization is ignored. Other than that, the model initial condition and model configuration are identical to those of CNTL. In an effort to test the sensitivity of model-simulated rainstorms to convective parameterization, we replace the Grell scheme of the CNTL with the Kain–Fritsch scheme (Kain and Fritsch 1993) in the third experiment (called KF54). The last experiment is the same as KF54, except that the 18-km grid (D03) is activated (KF18). A comparison between KF54 and KF18 will show the impact of grid resolution on the model simulation.

3. Synoptic situation

At 500 hPa, 0000 UTC 12 June 1991 (Fig. 3a), the ridge line of a strong western Pacific subtropical high pressure (WPSH) was located between 22° and 25°N. The 5880-gpm height contour, which is often used by Chinese meteorologists to identify the periphery of the WPSH, extended to 110°E and 22°N. Strong southwesterly flow appeared on the west and northwest sides of the WPSH. In middle latitudes, a major trough was located over northeastern China and the Yellow Sea. The southern part of the trough was oriented east-northeast–west-southwest, forming a weak cyclonic shear line along the Jiang-Huai Basin. Further to the west,

[2] The loci of upper-air soundings between 25° and 35°N are also plotted in Fig. 5. About five to six soundings are located in the vicinity of the cloud cluster D, suggesting that the rawinsonde network is capable of resolving the large meso-α-scale aspects of the cluster D.

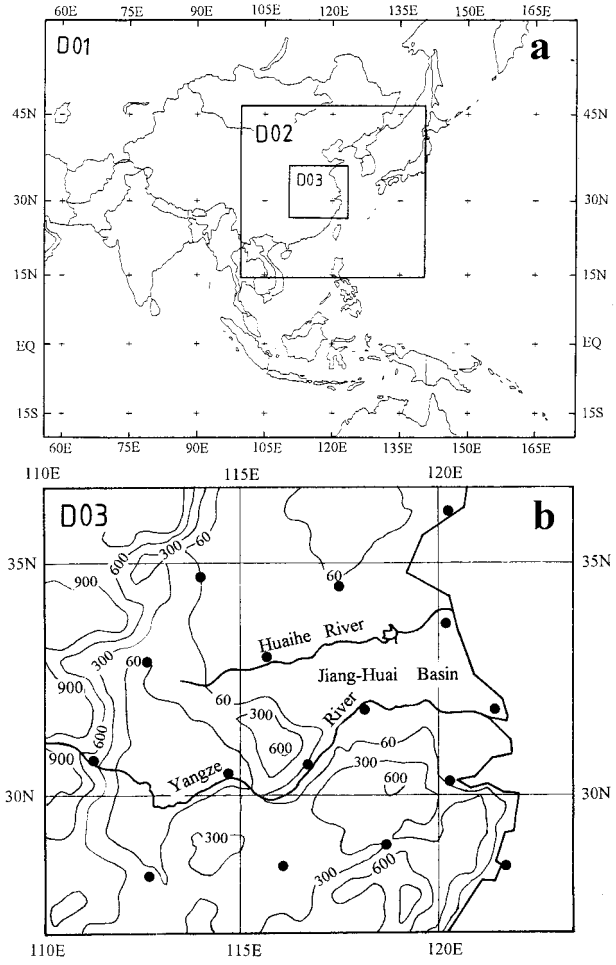

FIG. 2. (a) The model domains. (b) Geographical locations in domain 3 with solid dots marking the radiosonde locations. Terrain heights are contoured at 300-m intervals.

there was another shortwave trough, located along 105° E, with weak cold air advection behind it. The shear line over the Jiang-Huai Basin was more evident at 850 hPa (Fig. 3c). South of this shear line, there was a southwesterly synoptic-scale LLJ with wind speeds over 12 m s^{-1} extending from the South China Sea to the Jiang-Huai Basin. In the next 24 h (Fig. 3b) the shortwave trough moved very slowly, extending its base southeastward to merge with the shear line. A synoptic-scale omega pattern formed over central China with an anticyclone over the Yellow River valley (35°N, 113°E) and a trough on the east and west sides, respectively. The shear line between the Yellow River anticyclone to the north and the WPSH to the south was enhanced (Fig. 3d). This is a typical synoptic pattern accompanying heavy precipitation events in the Mei-Yu season (Ding 1992).

Figure 4a shows the 850-hPa streamlines and isotachs at 0000 UTC 12 June based on the model initial conditions. The southwesterly flow appears as a broad synoptic-scale LLJ with wind speeds greater than 12 m s^{-1} from southern China to southern Japan. The anticyclone to the north and the subtropical high to the south of the shear line helped produce a deformation field favorable for the low-level frontogenesis. A Mei-Yu front developed along the shear line with a θ_e gradient of about 8 K 100 km^{-1} (Fig. 4b). The 340-K θ_e contour can be used to represent the southern boundary of the Mei-Yu front. Very warm, moist ($\theta_e > 340$ K), and potentially unstable ($-\partial\theta_e/\partial p < 0$) air south of the front provided a favorable environment for the onset of the heavy precipitation. At this time, however, there were no mesoscale disturbances along the Mei-Yu front. The relative vorticity (ζ) along the shear line was rather weak (Fig. 4c), typically in the range of 3–5 $\times$ 10^{-5} s^{-1}.

A synoptic-scale vortex was located over southwestern China (32°N, 106°E; Fig. 3c). This vortex, known as the southwest (SW) vortex in China, is a significant rain-bearing system in the Mei-Yu season (Kuo et al. 1986; Ding 1992). In this case, the SW vortex remained nearly stationary from 0000 UTC 12 June to 0000 UTC 13 June 1991 (Fig. 3d). Convective cloud clusters generated in the vicinity of the SW vortex moved eastward, causing heavy precipitation in the Jiang-Huai Basin.

Mesoscale convective cloud clusters observed during this period have been analyzed by Li et al. (1993). Figure 5 illustrates the temporal evolution of cloud clusters along the 25°–35°N lat belt. At 0000 UTC 12 June, a major MCS,[3] labeled D, which had a diameter of 5.5° lat, was located at 29°–34°N, 104°–109°E. MCS D developed within the SW vortex. It is well known that the SW vortex is a trigger of convective systems along the Mei-Yu front in the summertime. Convective cloud clusters generated within the vortex often move eastward along the Mei-Yu front and cause heavy rainfall downstream (Zhu et al. 1981). Four small convective systems were observed east of MCS D at 0000 UTC 12 June, but only one cloud cluster, A′, began to develop to the northeast of D at 0400 UTC 12 June. Cloud cluster A′ moved eastward and intensified into a well-defined MCS by 1200 UTC. The area with T_{bb} (blackbody temperature) less than −54°C reached nearly 10^5 km^2. A second cloud cluster, B′, initiated at 1200 UTC 150 km to the east of A′, grew to its maximum intensity at 2000 UTC. During the development of A′ and B′, the MCS D was becoming progressively weaker and finally dissipated by 1800 UTC. At the same time, a new cloud cluster, D′, began to get organized to the south of the SW vortex and moved eastward.

The satellite picture at 1200 UTC 12 June (Fig. 6) shows a series of cloud bands located between 20° and 30°N, to the south of the cloud clusters D, A′, and B′ along the Mei-Yu front. These cloud bands originated

[3] At 850 hPa, a warm, moist center with $\theta_e > 354$ K in the initial condition was associated with MCS D, suggesting that some aspects of the meso-α-scale environment of MCS D were included in the model initial condition.

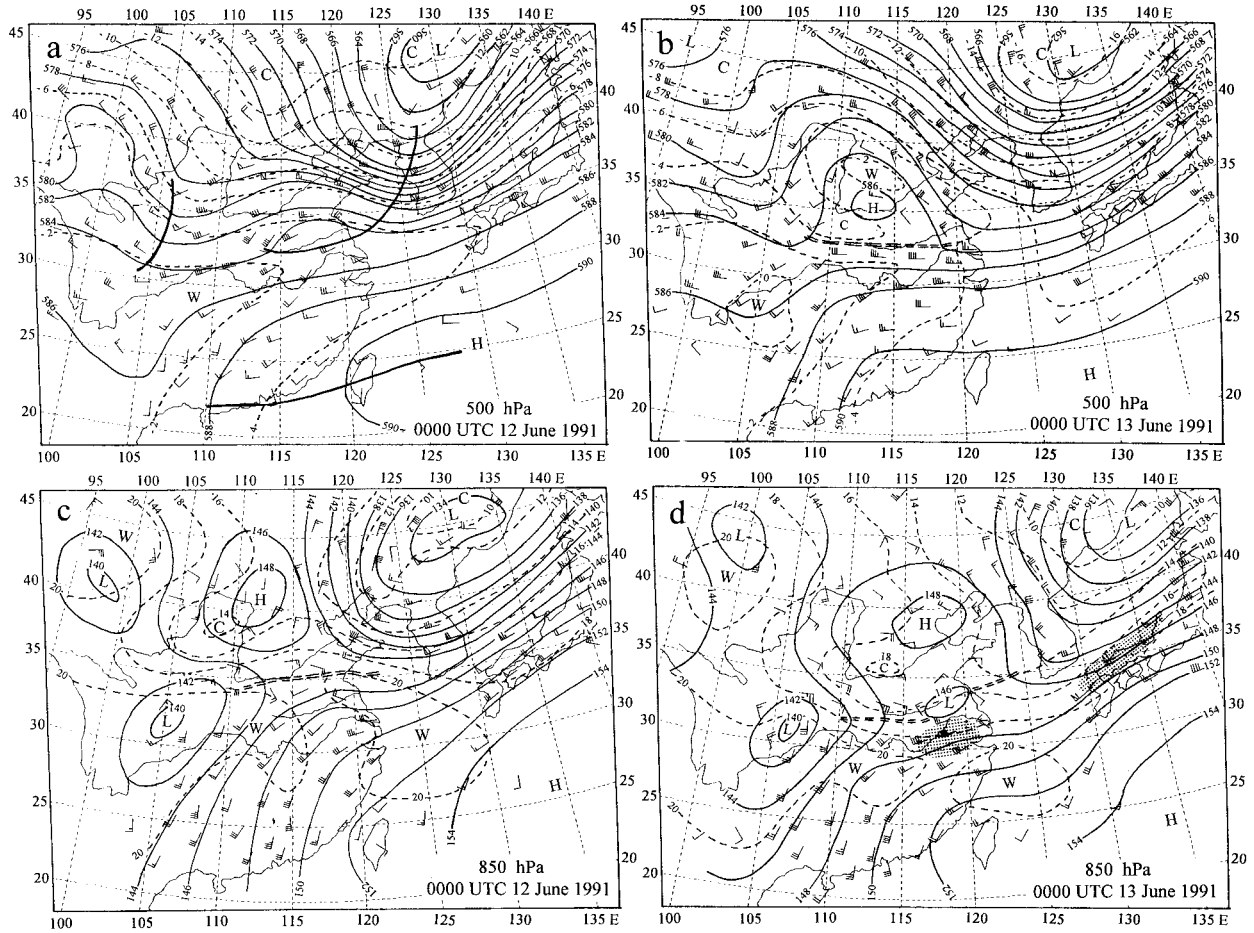

FIG. 3. Manual analyses of the geopotential height (every 20 gpm) and temperature (every 2°C) fields at (a) 500 hPa, 0000 UTC 12 June 1991; (b) 500 hPa, 0000 UTC 13 June 1991; (c) 850 hPa, 0000 UTC 12 June 1991; and (d) 850 hPa, 0000 UTC 13 June 1991. Thick solid lines depict trough lines and the ridge line (WPSH), double dashed lines represent shear lines. Observed winds are plotted. Areas of wind speeds over 16 m s^{-1} are shaded in (d) to verify the model results shown in Fig. 7.

in the South China Sea and were associated with the strong southwesterly flow at 850 hPa (Figs. 3c and 3d). As cloud cluster A′ reached its mature stage at 1200 UTC 12 June, cloud cluster B′ was being organized 150 km to the east of A′. These two eastward moving MCSs were responsible for the heavy flooding in the Jiang-Huai Basin.

By 0000 UTC 13 June, a meso-α-scale low (32°N, 118°E) at 850 hPa had formed over the Jiang-Huai Basin (Fig. 3d). Heavy precipitation occurred at the southeastern part of this low. An LLJ with wind speeds in excess of 16 m s^{-1} was observed over the lower Yangzi River valley. Another LLJ with maximum speed of 24 m s^{-1} was located over southern Japan. Due to the lack of upper-air observations over the East China Sea, it is not clear if there was another LLJ streak over the ocean.

From the aforementioned synoptic description, the key features of this heavy rainfall case can be summarized as the following:

1) successive development of rainstorms along the Mei-Yu front,
2) development of the mesoscale LLJ to the south of the rainstorms,
3) development of a meso-α-scale low associated with the rainstorm, and
4) heavy precipitation over the Jiang-Huai Basin caused by the successive eastward propagation of mesoscale convective systems.

4. Overview of the model results

The 24-h accumulated rainfall over the Jiang-Huai Basin simulated by the 54-km CNTL experiment is shown in Fig. 1b. Generally speaking, the model captured the main features of the observed heavy rainfall in terms of location and intensity. The model rainfall was concentrated along a zone 1000 km long and 250 km wide, about 100 km north of the observed area. Three heavy rainfall centers were simulated in the rain belt. The west center (32°N, 112°E) was about 150 km north of the observed, but the intensity was similar. The rainfall center simulated at 32.5°N, 113.5°E was at the

right location but the intensity was overpredicted. Figure 1c shows the partitioning of model precipitation into resolvable-scale and subgrid-scale components. The results indicate that most of the precipitation (~90%) was produced by the resolvable-scale circulation. Subgrid-scale convective rainfall was relatively small and occurred on the southern edge of the rainfall belt. Precipitation produced by the subgrid-scale convective parameterization in the lower Yangzi River valley along 32°N reached 44 mm, where the storms A′ and B′ occurred (Fig. 5). In this area, convective rainfall was about 30%–50% of the total precipitation. Further discussion of this subject will be presented in section 5g. The simulated 6-h (1200–1800 UTC 12 June, Fig. 1f) rainfall region was also 100–150 km north of the observed, although the total amounts were about the same. These are encouraging results for a model with a 54-km grid. The rest of the paper will focus on the analysis of the 54-km CNTL simulation.

Three main rainstorms were simulated at 0000 UTC 13 June[4] (Fig. 7a). Two rainstorms (labeled A and B, respectively) were simulated over China, and the third, labeled C, was simulated over Japan.[5] All of these storms are located at the southern edge of the Mei-Yu front in a very warm, moist air mass with θ_e's above 340 K (Fig. 7b) and water vapor mixing ratios over 15 g kg^{-1}. High cyclonic relative vorticity (ζ) is associated with rainstorms A and B, reaching 3.3×10^{-4} s^{-1} and 2.4×10^{-4} s^{-1} at 850 hPa, respectively (Fig. 7c). A vorticity center is not collocated with storm C, possibly due to differences in the Mei-Yu frontal structure over China and Japan (Kato 1985). The values of these three vorticity maxima are an order of magnitude greater than those of synoptic-scale systems (Fig. 4c). The vorticity maxima, as well as the rainstorms, exhibit a wavelength of approximately 400 km. Ogura et al. (1982) found a similar wavelength for mesoscale disturbances in the divergence field along a cold front case in the 1979 Severe Environmental Storms and Mesoscale Experiment.

Figure 8 shows the temporal evolution (at 3-h intervals) of the model hourly rainfall. The transient nature of the rainstorms is evident. Four rainstorms were simulated within 24 h. The first storm, labeled as S, was initiated at $t = 3$ h (32°N, 110°E) and reached its maximum intensity at $t = 6$ h, after which time it weakened quickly. Its lifetime was only 7 h. Storm A formed to the east of storm S at $t = 5$ h and reached its peak intensity at $t = 9$ h, with a 1-h rainfall of 52.5 mm. At $t = 12$ h (1200 UTC 12 June), storm A was still in its mature stage (1-h rainfall of 32.7 mm). A new storm, labeled B, started to develop 150 km to the east (downstream) of storm A at $t = 10$ h (also see Fig. 13h) and reached its maximum intensity at $t = 21$ h, with an hourly rainfall of 21.5 mm. Storm C formed at $t = 15$ h and was not as intense as A or B. NO91 also simulated the transient nature of rainstorms (which they referred to as convective precipitation systems), although in their simulations new storms developed on the west side (upstream) of the preceding storm.

Unfortunately, the lack of hourly rainfall data over our study area prevents us from directly verifying the model hourly rainfall. Statistical studies of the relationship between T_{bb} and hourly rainfall in the Mei-Yu season (Xiang et al. 1993) have shown that about 75% of stations record hourly precipitation greater than 5 mm when T_{bb} is less than −60°C. Thus, the evolution of MCSs from satellite images can be used to verify the numerical results. The temporal variation of MCSs in Fig. 5 shows that the MCSs A′ and B′ moved in the same directions as the model rainstorms A and B, but that the positions of the observed storms were about 200–300 km south of the simulated rainstorms. This discrepancy is consistent with the observed precipitation areas (Figs. 1a and 1e) being south of those simulated (Figs. 1b and 1f).

One of the most interesting features is the development of three mesoscale wind maxima in the broad southwesterly flow at 850 hPa, south of the rainstorms at $t = 24$ h (Fig. 7a). These mesoscale wind maxima are also simulated at 700 and 500 hPa (not shown). The strong wind streaks can be regarded as mesoscale disturbances associated with the rainstorms and are referred to as mesoscale low-level jets (for simplicity, we will refer to these as mLLJs). The existence of these mLLJs are supported by the available wind observations shown in Fig. 3d. Over the continent, the simulated mLLJ is about 150 km north of that observed and is 6–8 m s^{-1} stronger. The simulated mLLJ over the Japanese islands is nearly perfect in terms of position and intensity. The mLLJ over the East China Sea cannot be verified due to the lack of upper-air observations in this region.

A meso-α-scale low was simulated over the Jiang-Huai Basin (118°E, 32.5°N) at 0000 UTC 13 June. The position of the simulated mesolow and the shear line associated with the Mei-Yu front (Fig. 7a) also appeared 150 km north of those observed, which is consistent with the position errors of the simulated rainstorms as mentioned earlier. The intensity of the model mesolow is 20 gpm deeper than the observations (Fig. 3d). A detailed discussion of this mesolow will be presented in the next section.

5. The rainstorm, mLLJ, and meso-α-scale low

a. The rainstorm and mesoscale low-level jet

The simulation of storm A at $t = 12$ h (1200 UTC 12 June) will be analyzed in this section since this storm was the main rain-bearing system in this case and also because observations are available for its verification.

[4] There was a fourth rainstorm (labeled as S in Fig. 8) simulated in the model, but it only lasted for about 7 h.

[5] Storm C will not be analyzed or discussed in this paper.

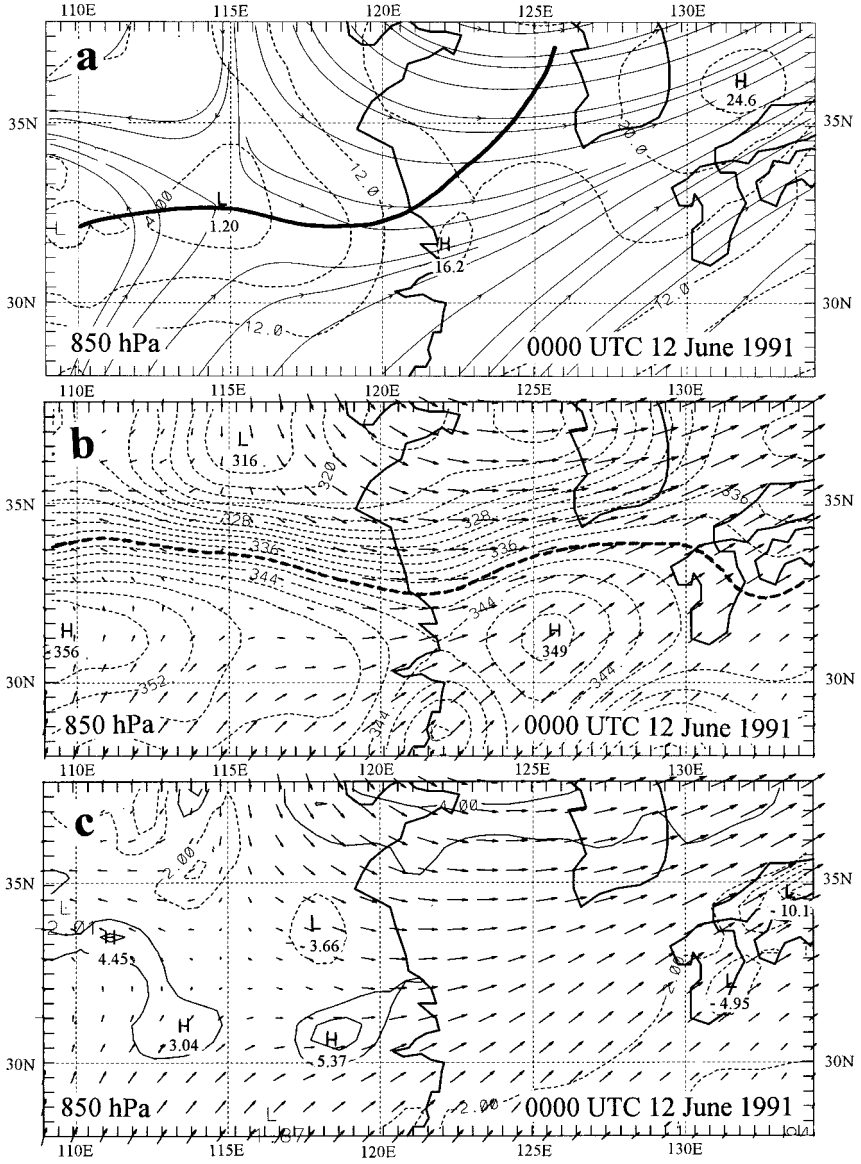

FIG. 4. Model initial condition for 850 hPa at 0000 UTC 12 June 1991. (a) Streamlines and isotachs (dashed lines every 4 m s^{-1}). Thick line represents trough or shear line. (b) Equivalent potential temperature θ_e (dashed lines every 2 K) and wind vectors. The contour of θ_e = 340 K is highlighted to indicate the southern boundary of the Mei-Yu front. (c) Wind vectors and relative vorticity (contour interval 2 × 10^{-5} s^{-1} with 0 line omitted).

Figure 9 compares the 1-h rainfall (over 10 mm) from the observations (shaded area[6]) with the model simulation (in contours). The 850-mb model streamline provides a background to show the location of the rainstorm relative to the Mei-Yu shear line and the cyclonic circulation associated with the mesolow. The simulated rainfall amount of 32.7 mm compares very well with the observed value of 36.5 mm. The model rainstorm's position, however, is about 150 km (approximately three grid points) north of the observation.

Figure 10a shows the simulated low-level (850 hPa) wind and height fields at t = 12 h and reveals that a mesoscale low is collocated with the convective system A. This mesoscale low first appears at t = 6 h along the shear line to the east of the SW vortex (not shown) 3 h after the onset of heavy rainfall. This suggests that the pressure drop is a result of latent heat release. Concurrent with the development of storm A, this mesolow intensifies and moves eastward. Cyclonic circulation intensifies with the development of the mesolow. By t =

[6] The hourly rainfall data east of 115°E are not available.

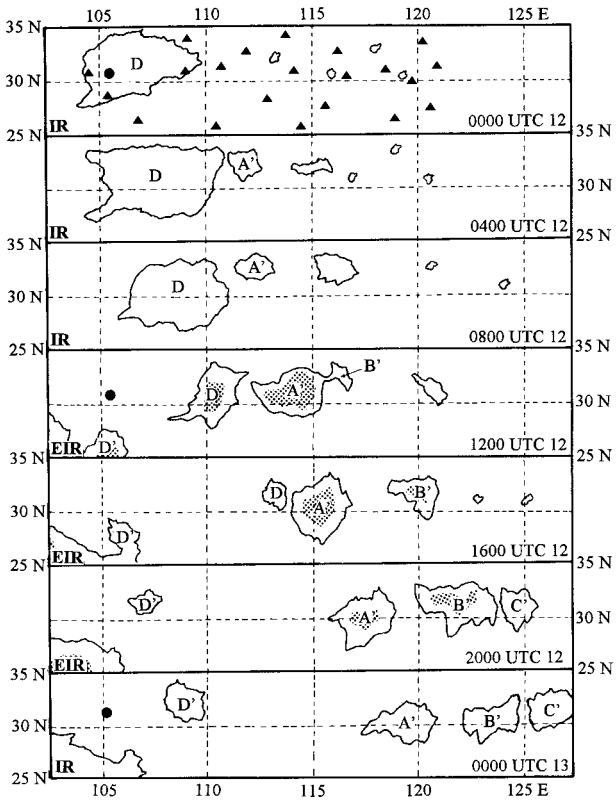

FIG. 5. Temporal variation of cloud clusters (25°–35°N, 100°–125°E) every 4 h from 0000 UTC 12 June to 0000 UTC 13 June 1991. The cloud clusters of 0000–0800 UTC 12 June and 0000 UTC 13 June are from IR images, whereas 1200–2000 UTC 12 June are from enhanced IR (EIR) images. The areas of T_{bb} lower than −54°C are shaded. Black dots indicate the position of the SW vortex. Triangles in the top figure depict radiosonde locations. The cloud clusters of interest are labeled. Latitudes are labeled at the left and right sides alternately for different panels [adapted from Li et al. (1993)].

18 h, a closed vortex forms. It becomes well defined at $t = 24$ h (Fig. 7a).

The most important feature in the simulation is the mLLJ, with a horizontal scale of a few hundred kilometers and a maximum speed of 20 m s^{-1}, located to the south of the storm. A similar mLLJ was simulated by NO91 in a case of heavy precipitation over southern Japan in the Baiu season. To verify the simulation, all available wind observations at 1200 UTC 12 June are plotted in Fig. 10a. Both the observed and simulated wind fields show cyclonic shear around the mesolow, but without a closed vortex. It should be pointed out that the station between storms A′ and B′ observed a 4 m s^{-1} northerly wind, indicating cyclonic circulation associated with the rainstorm B′ to the east of this wind observation, although the simulated wind is southerly (no cyclone to the east). The surface analysis by the National Meteorological Center of China indicated a weak low associated with rainstorm B′ (not shown). Except for this discrepancy, there is no significant error in the simulated wind field (i.e., the model wind speeds are generally within 2 m s^{-1} of those observed). Unfortunately, the observations are not of sufficient density to verify the existence of the simulated mesoscale wind structure, and thus the exact position of the mLLJ streak cannot be verified.

The simulated mLLJ is highly ageostrophic, with southwesterly winds crossing the height contours toward the low. The mLLJ accelerates northward and injects warm, moist air into the storm.

At 300 hPa (Fig. 10b), mesoscale wind disturbances are also simulated. A wind speed maximum (greater than 20 m s^{-1}) is located ahead (east) of storm A. The observed wind speeds near this wind maximum are also 20 m s^{-1}. West of storm A, a westerly wind speed of

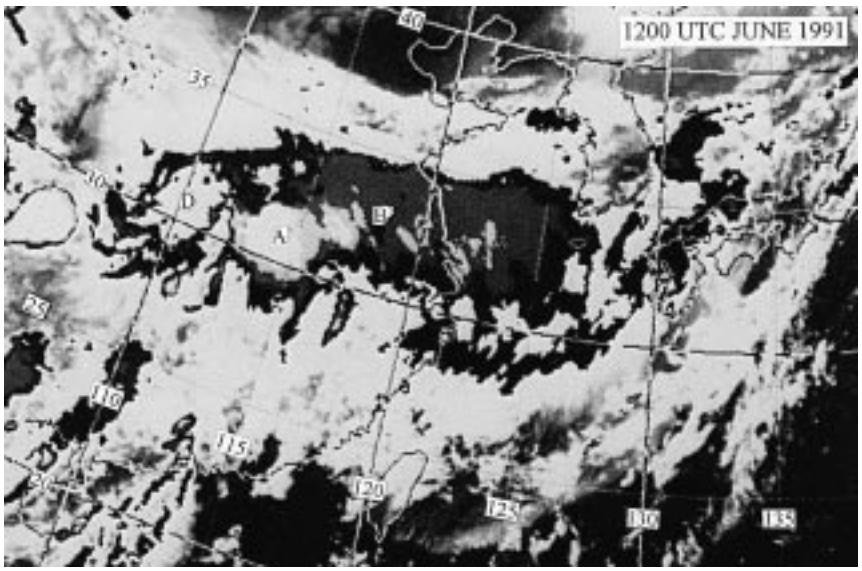

FIG. 6. EIR satellite images at 1200 UTC 12 June 1991. The white areas labeled as D, A′, and B′ are the MCSs with T_{bb} less than −54°C.

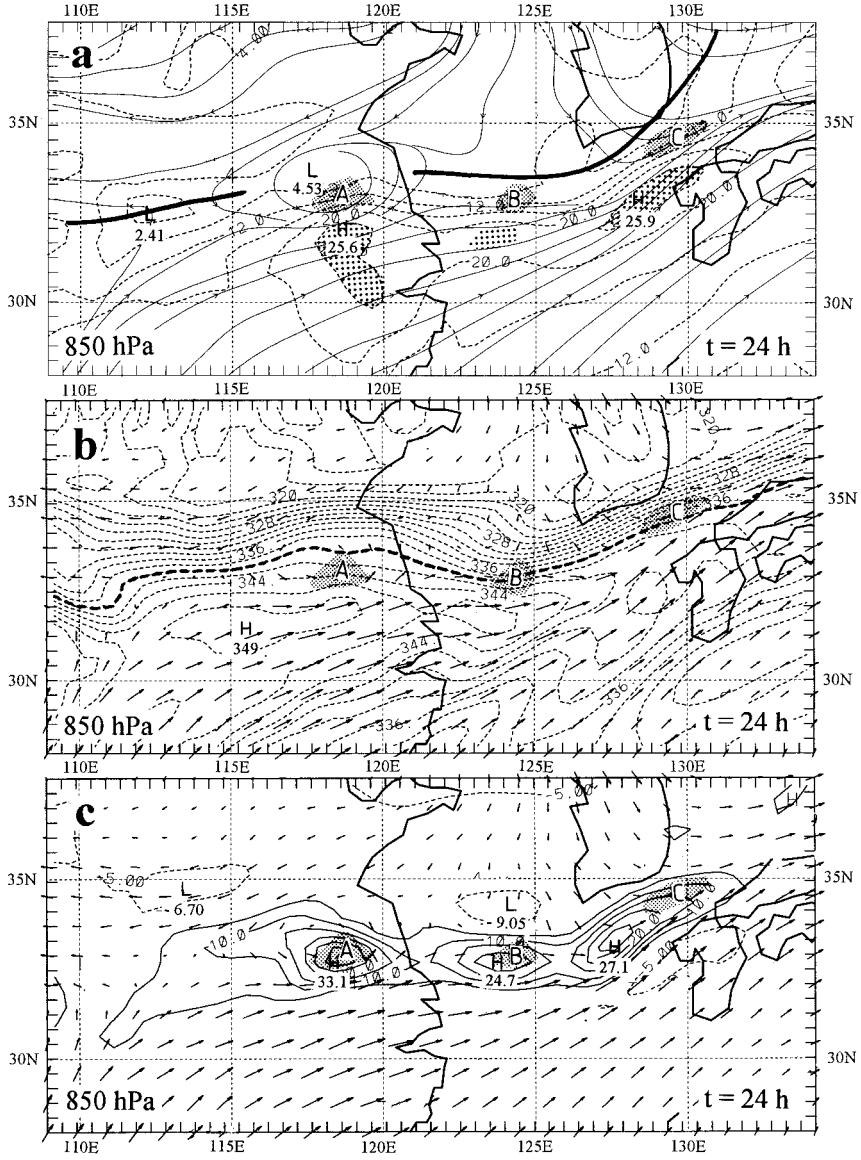

FIG. 7. Simulated 850-hPa fields at $t = 24$ h (valid at 0000 UTC 13 June 1991). (a) Streamlines (solid) and isotachs (dashed, every 4 m s^{-1}). Thick line represents trough or shear line. Areas of wind speeds greater than 24 m s^{-1} are stippled. (b) Equivalent potential temperature (θ_e, dashed lines every 2 K) and wind vectors. The contour of $\theta_e = 340$ K is highlighted to indicate the southern boundary of the Mei-Yu front. (c) Relative vorticity (solid lines, contour interval 5×10^{-5} s^{-1}) and wind vectors. Areas of 1-h rainfall ($t = 23$–24 h) greater than 10 mm are shaded and labeled as A, B, and C to indicate the rainstorms simulated at $t = 24$ h.

13 m s^{-1} is observed. An increase in wind speed through storm A is evident both in the observation and the simulation. Similarly, strong winds (>20 m s^{-1}) to the east and weak winds (~11 m s^{-1}) to the west of storm B are also simulated. Although it may not be appropriate to call this wind maximum a mesoscale upper-level jet at this time, the maximum between storms A and B did develop into a mesoscale jet at $t = 24$ h (see Fig. 14c). The wind vectors are diffluent over the rainstorms A and B. The upper-level divergence reaches 16×10^{-5} s^{-1} over model rainstorm A (see Fig. 14d), associated with the upper-level outflow of the rainstorm.

b. Vertical structure of the rainstorm

Figure 11 presents vertical cross sections through rainstorm A. The region of rainwater concentration greater than 0.4 g kg^{-1} is used to represent the rainstorm. The Mei-Yu front is confined to below 700 hPa with a weak potential temperature gradient [~1 K (100 km)$^{-1}$,

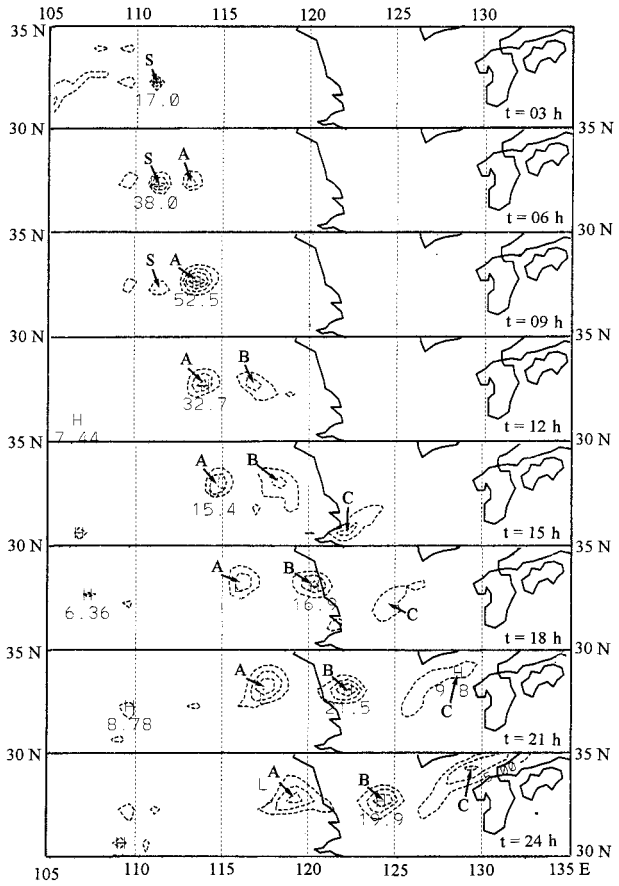

FIG. 8. Simulated hourly rainfall at 3-h intervals from $t = 3$ h (0300 UTC 12 June) to $t = 24$ h (0000 UTC 13 June 1991). Isohyets are every 5 mm for $t = 3$ h (0300 UTC 12 June) and $t = 15$ h to 24 h (1500 UTC to 0000 UTC 13 June) and 10 mm for $t = 6$ h to 12 h (0600 UTC to 1200 UTC 12 June). Latitudes are labeled at the left and right sides alternately for different panels.

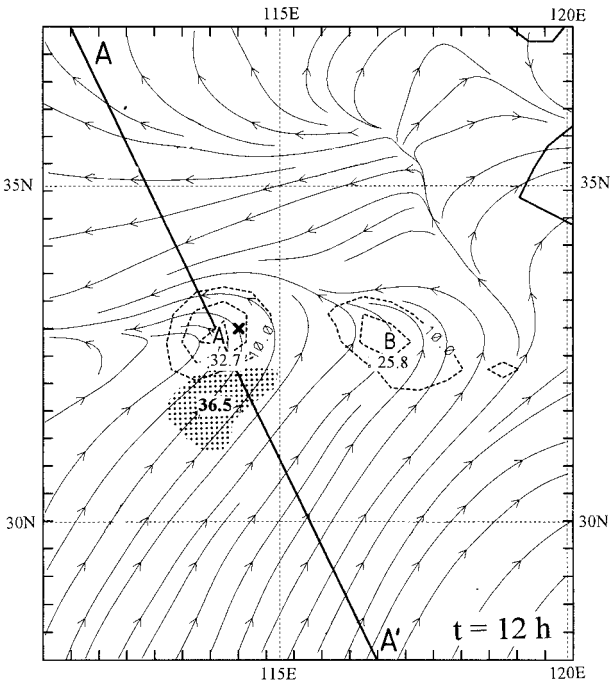

FIG. 9. Simulated 1-h precipitation ($t = 11$–12 h, dashed lines every 10 mm, maximum rainfall 32.7 mm) and 850-hPa streamlines at $t = 12$ h (1200 UTC 12 June). The observed 1-h rainfall area greater than 10 mm is stippled (maximum rainfall 36.5 mm). The thick solid line AA′ shows the position of the vertical cross sections shown in Fig. 11, and X indicates the position of the model sounding shown in Fig. 17.

Fig. 11a], but strong θ_e gradient [$\sim$15 K (100 km)$^{-1}$ at 900 hPa, Fig. 11b]. The mixing ratio is 18 g kg^{-1} in the warm air and 6 g kg^{-1} in the cold air (Fig. 11c), showing a strong contrast of moisture. This moisture contrast across the Mei-Yu front is similar to that found by Ma and Bosart (1987). Warm, moist air with θ_e greater than 350 K in the boundary layer to the south of the front appears to be the main energy source driving the rainstorms. The atmosphere is moist neutral to potentially unstable to upright convection from 900 to 400 hPa above the front.

Even at the mature stage of rainstorm A, the mLLJ remained highly unbalanced. Distinct vertical wind shear ($\sim$15 m s^{-1} km^{-1}) of the mLLJ is simulated below 700 hPa. Compared with the thermal wind of $\sim$5 m s^{-1} km^{-1} [calculated using a temperature gradient of 1 K (100 km)$^{-1}$], this mLLJ is considerably stronger than the thermal wind. To achieve a new geostrophic balance, upward (downward) motion should be induced on the north (south) side of the vertical wind shear to increase the temperature gradient (Holton 1990). Therefore, an indirect circulation has to be established in order to restore the dynamic balance. Figure 11d shows the upward motion in the rainstorm area, immediately to the north of the mLLJ, with a maximum of $\sim$70 cm s^{-1}. This is very strong vertical velocity for a 54-km model. It should be pointed out that such a strong vertical velocity is not purely the result of dynamic forcing. Latent heat release associated with the rainstorm has to be a major contributor. As will be shown later in section 5f, the maximum vertical velocity is reduced to 6 cm s^{-1} when latent heat release is suppressed. Although most of the upward vertical motion can be accounted for by latent heat release associated with the rainstorms, the dynamic forcing can be an important factor for initiating the development of the rainstorms. The vectors along the cross section show intense low-level inflow below 850 hPa and outflow above 300 hPa. Downward motion south of the rainstorm is not as pronounced as the upward motion because it occurs over a much broader area. A secondary circulation, associated with convection, with upward motion to the north, and very weak downward motion to the south of the mLLJ is simulated (Fig. 11d). Chou et al. (1990) simulated a similar circulation in a two-dimensional model of Mei-Yu frontogenesis. Chen et al. (1998) also found this kind of vertical circulation with less intensity along the LLJ in a heavy precipitation case that occurred in Taiwan.

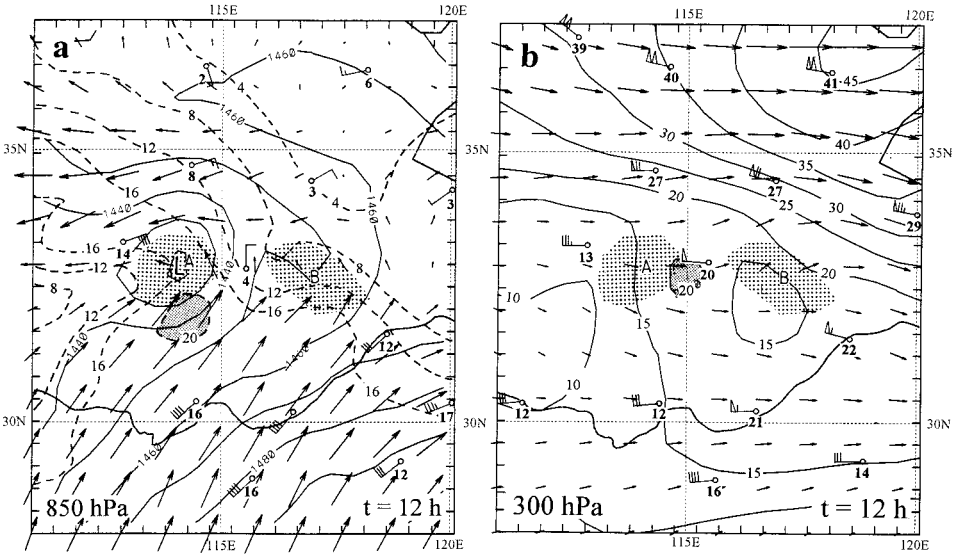

FIG. 10. Simulated fields at $t = 12$ h (1200 UTC 12 June 1991). (a) The 850-hPa geopotential height (thin solid lines every 10 gpm), wind vector, and wind speed (dashed lines every 4 m s^{-1}). (b) The 300-hPa wind vector and isotachs (solid lines every 5 m s^{-1}). Simulated hourly rainfall areas greater than 10 mm are stippled. Labels A and B indicate the rainstorms. Areas of model wind speeds greater than 20 m s^{-1} at 850 and 300 hPa are shaded to show the LLJ and ULJ, respectively. The corresponding observed winds are plotted with the wind speed (bold, in m s^{-1}) marked at the base of the wind barbs.

Concurrent with the development of the mLLJ, an easterly jet formed at 950 hPa, north of the rainstorm (Fig. 11a). A direct circulation below 700 hPa can be found along this easterly LLJ (Fig. 11d). Chen et al. (1994) have diagnosed this direct circulation in a case during the Taiwan Area Mesoscale Experiment (Kuo and Chen 1990) IOP5.

High relative vorticity (ζ) and potential vorticity (PV) are associated with the rainstorm, with maximum values of 4.8×10^{-4} s^{-1} and 3 PVU (1 PVU = 10^{-6} K kg^{-1} m s^{-1}) at ~800 hPa, respectively (Figs. 11e and 11f). These high ζ and PV appear with the rainstorm A at $t = 6$ h (not shown) and intensifies rapidly as the rainstorm develops. It is evident that this high PV is associated with the latent heat release in the rainstorm area.

c. Trajectory analyses

To give a comprehensive picture of the three-dimensional airflow around the rainstorm, a number of trajectories are calculated. These are prepared with a time step of 0.5 h using the Vis5D software developed by Hibbard and Santek (1990). Figure 12a depicts two groups of trajectories, one originating from the warm, moist air (parcels W_1 and W_2) and the other originating from the cold, dry air (parcels C_1, C_2, and C_3). It is evident that the rainstorm is fed by a southerly flow of convectively unstable air. Parcel W_1 begins at 1.5 km in the convectively unstable area. It moves northeastward across the 850-hPa height contours and the mLLJ core, and penetrates into the rainstorm. It rises abruptly after $t = 9$ h, climbs to 10 km by $t = 15$ h, reaching the level of upper-level northwesterly. Parcel W_1 then turns southeastward, maintaining a slight ascending motion in the upper troposphere. The trajectory of parcel W_2 is similar to that of W_1, but W_2's maximum elevation is 1–2 km lower than that of W_1. Parcel W_2 turns to the south in a more pronounced way than W_1.

The low-level cold, dry air to the north of the rainstorm was descending. Parcel C_1 originated at 3 km, moved southeastward, and descended to 2.2 km by $t = 12$ h. It then turned to the west anticyclonically and descended farther down to 0.9 km by $t = 18$ h. Parcel C_2 moved southeastward and descended from 3.0 km to 2.5 km in the first 6 h, then moved eastward at near constant elevation. Parcel C_3 descended 1.1 km (from 2.8 km to 1.7 km) in the first 12 h and then turned to the northwest while continuing to descend. Using the $\theta_e = 340$ K contour to locate the Mei-Yu front, it is found that the warm, moist air originating from the southwest was forced to rise over the frontal surface. Trajectories in the cold air fanned out on the north side of the front. The descending cold air (C_1, C_2, and C_3) met with the southwesterly warm air (W_1 and W_2) and resulted in strong convergence along the front. If we project W_1, W_2 and C_1, C_3 on a y–z plane (Fig. 12b), a Lagrangian circulation along the mLLJ is evident. This is similar to the vertical circulation presented in Fig. 11f. The vertical circulation along mLLJ existed both in a Eulerian and a Lagrangian framework.

d. Evolution of the mesoscale low-level jet

The relationship between the rainstorm and the mLLJ needs to be further clarified. Is the mLLJ a cause or a

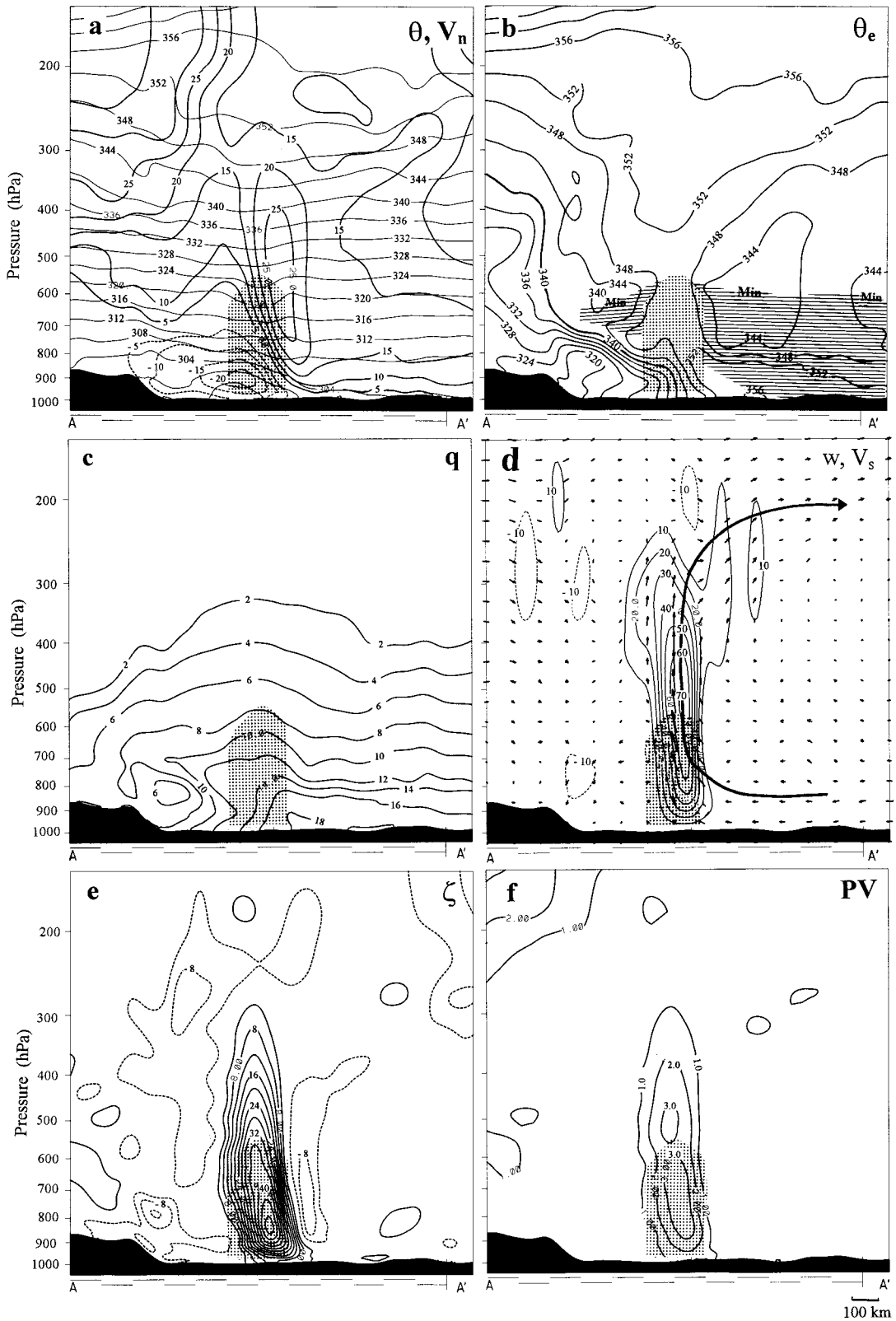

FIG. 11. Vertical cross sections along line AA′ in Fig. 9 for $t = 12$ h simulation. Stippled areas indicate rainwater greater than 0.4 g kg^{-1} in rainstorm. (a) Potential temperature (q, thin lines every 4 K) and wind speed normal to the cross section (V_n, thick lines every 5 m s^{-1}). (b) Equivalent potential temperature θ_e (every 4 K) with hatched area indicating convective instability ($-\partial\theta_e/\partial p < 0$). (c) Mixing ratio, q (every 2 g kg^{-1}). (d) Vertical velocity (every 10 cm s^{-1}) and in-plane vertical circulation with heavy arrow indicating representative streamline along the plane. (e) Relative vorticity (ζ, every 4×10^{-5} s^{-1}). (f) Potential vorticity PV (in PV unit, 1 PV unit = 10^{-6} K kg^{-1} m s^{-1}).

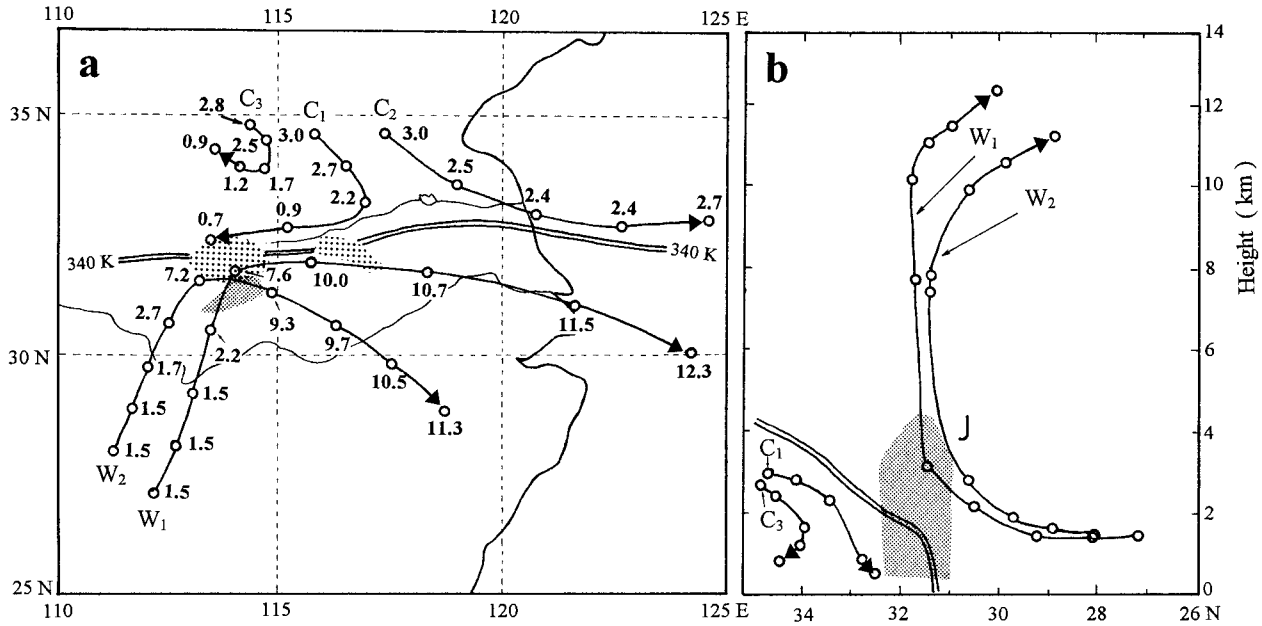

FIG. 12. (a) Two groups of forward trajectories from $t = 0$ h to $t = 24$ h: one from the warm and moist air—W_1 and W_2; the other from the cold and dry air—C_1, C_2, and C_3. Vertical positions of the parcels (bold, in km) are indicated every 3 h (6 h) along the warm (cold) air trajectories. Rainstorms are stippled, and mLLJ is shaded. (b) Trajectories on the y–z plane for parcels W_1, W_2, and C_1, C_3. Double line depicts $\theta_e = 340$ K surface (representing the southern boundary of the Mei-Yu front), shaded area indicates rainwater greater than 0.4 g kg^{-1}, and "J" the LLJ on the y–z plane at $t = 12$ h.

consequence of the convection? To answer this question, we examine the evolution of the rainstorms and the wind fields at 850 hPa from hourly model output (Fig. 13).

At $t = 3$ h, the wind speeds around storm S, which was just initiated, were about 8 m s^{-1}. Although there was a relatively high speed immediately to the south of the storm, the mLLJ was not evident at this time (Fig. 13a). It should be noted that the southerly flow at the tip of this wind speed maximum was directed toward the rainstorm, which means that the warm, moist air was being advected into the storm. One hour later, wind speeds to the southeast of this storm increased to 12 m s^{-1} and a jet streak appeared, signaling the formation of the mLLJ (Fig. 13b). At $t = 5$ h, associated with the development of storm S and the initiation of storm A to its east, the 12 m s^{-1} isotach split into two relative maxima to the south of these two storms (Fig. 13c). This mLLJ intensified to 16 m s^{-1} by $t = 6$ h (Fig. 13d). While storm S decayed at $t = 7$ h, storm A developed rapidly (Fig. 13e). The 16 m s^{-1} isotach penetrated into the storm A (Fig. 13f).

At $t = 9$ and 10 h, when storm A was mature, the mLLJ increased up to 20 m s^{-1}. The horizontal momentum of the mLLJ was concentrated in a narrow zone about 100 km wide (Figs. 13g and 13h). The height of the cloud base of the storm was about 900 hPa at this time. The volume of warm, moist air feeding into the storm increased rapidly in the mature stage. It should be noted that another wind speed maximum occurred to the east of the main mLLJ (31°N, 116°E) at $t = 9$ h. One hour later, storm B appeared[7] and the associated wind speed to its south also increased (Fig. 13h). As the southerly mLLJ penetrated into the storm, an easterly LLJ formed to the north of the storm. This easterly LLJ can be seen in the cross section through the storm in its mature stage (Fig. 11a).

Although the interaction between the rainstorm and mLLJ is not yet fully understood, the hourly model output shows that the mLLJ developed nearly simultaneously with the rainstorm. The latent heat release associated with the rainstorm produces pressure fall. The pressure fall then accelerates air parcels toward the low and creates the mLLJ. Strong convergence north of the mLLJ and the release of convective instability further enhance the rainstorm, as well as the mLLJ itself, establishing a positive feedback between mLLJ and the rainstorm.

Chen and Yu (1988) analyzed the relationship between heavy rainfall events and the synoptic-scale LLJ in the Taiwan area. About 84% of the heavy rainfall events were accompanied by a 700-hPa LLJ, which existed 12 h before the start of heavy rain. In our case, the synoptic-scale LLJ also existed before the development of the rainstorms (Fig. 3c and 4a). However, the mesoscale LLJ in our model simulation forms as a con-

[7] A rain cell of 5 mm h^{-1} (not yet reaching 10 mm) already existed at $t = 9$ h.

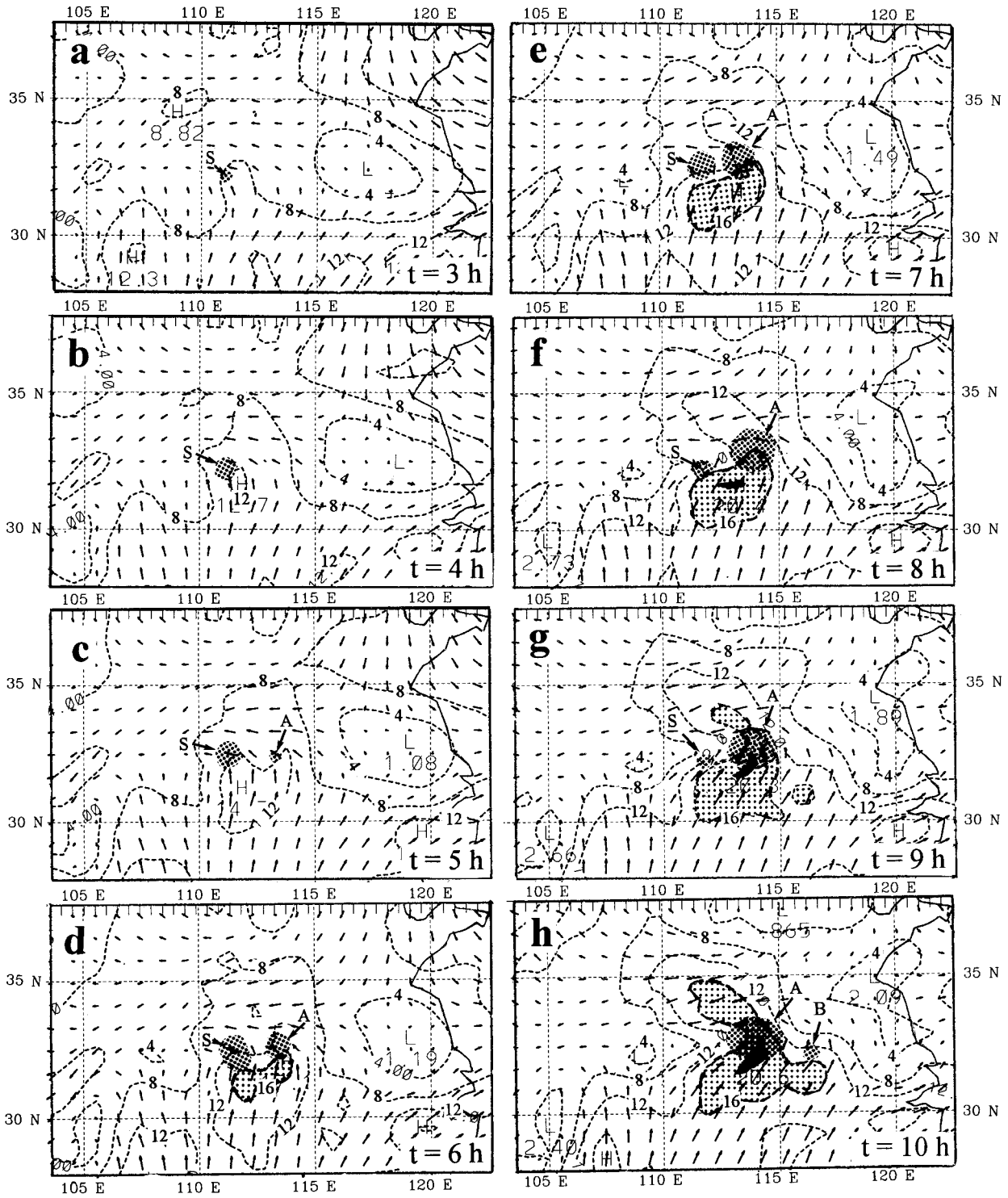

FIG. 13. Simulated 850-hPa wind vectors and speeds (dashed lines every 4 m s^{-1}) every hour from t = 3 h (0300 UTC 12 June) to t = 10 h (1000 UTC 12 June). Heavy-stippled areas depict rainstorms S and A, and light-stippled and black areas indicate the wind speeds greater than 16 and 20 m s^{-1}, respectively.

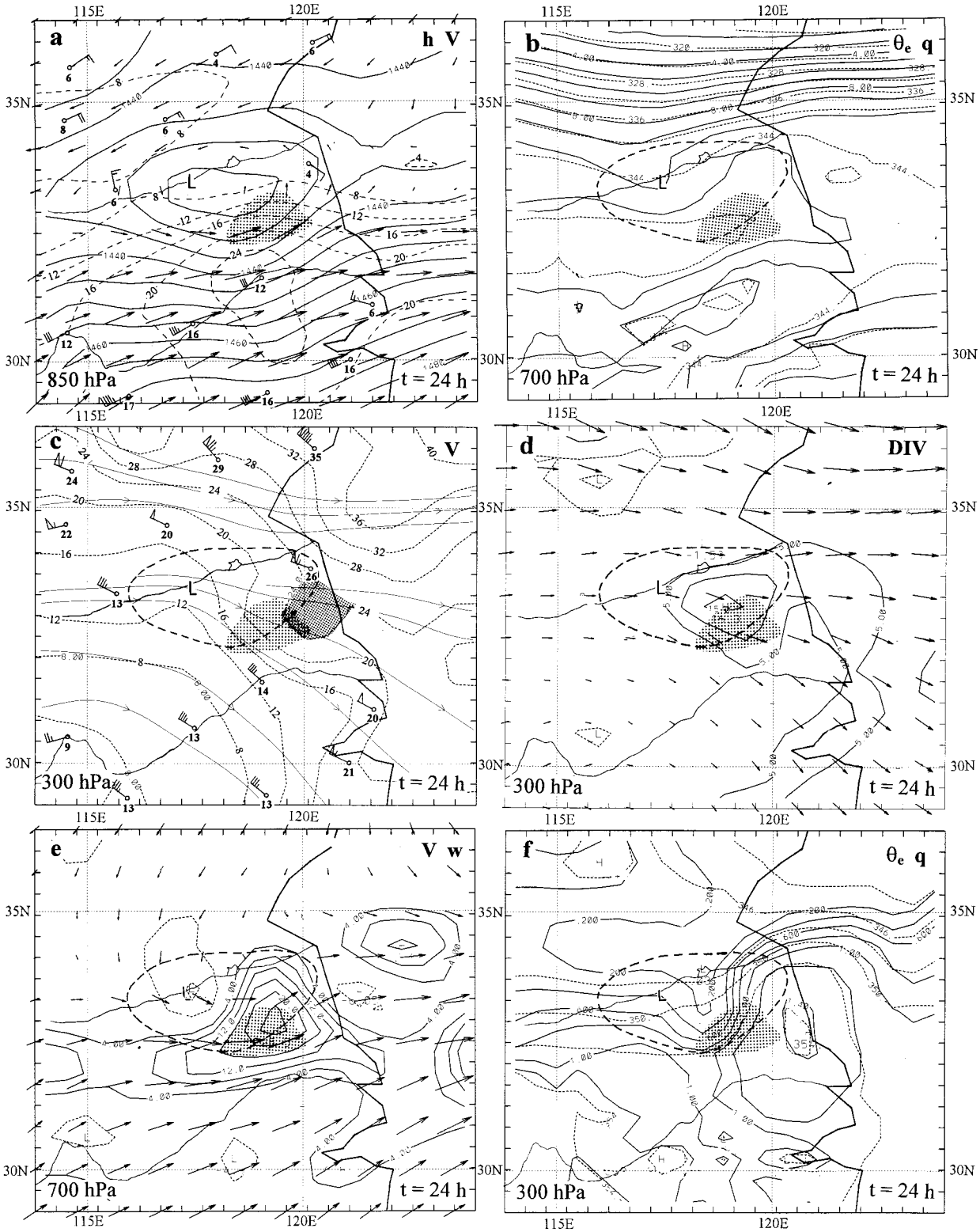

FIG. 14. Simulated meso-α-scale low at $t = 24$ h (0000 UTC 13 June 1991). (a) The 850-hPa geopotential height (solid lines every 10 gpm), wind vectors, and isotachs (dashed lines every 4 m s^{-1}). (b) The 700-hPa mixing ratio (solid lines every 1 g kg^{-1}) and θ_e (dashed lines every 4 K). (c) The 300-hPa streamlines (solid) and isotachs (dashed every 4 m s^{-1}) with wind speed over 24 m s^{-1} in ULJ shaded. (d) The 300-hPa divergence (every 5×10^{-5} s^{-1}, solid lines for divergence, and dashed lines for convergence). (e) Vertical velocity at 700 hPa (every 4 cm s^{-1}, solid lines for upward motion, and dashed lines for downward motion). (f) The 300-hPa mixing ratio (solid lines every

sequence of the rainstorm. Further study is needed to understand the multiscale interaction between the synoptic-scale LLJ, the mLLJ, and the rainstorm.

e. Mature stage of the mesolow

Although the meso-α-scale low appeared as early as $t = 6$ h, a closed vortex did not appear until $t = 24$ h. Figure 14a shows the wind and thermal fields of the simulated mesolow at $t = 24$ h. At 850 hPa, the height of the mesolow was 5 gpm higher than that at $t = 12$ h (not shown), but the speed of the mLLJ was increased by 4 m s^{-1}, clearly showing the mutual adjustment between the wind and pressure fields, which led to the decrease of the pressure gradient and an increase in wind speed. The major difference between observations and the simulation is the strength of the mLLJ. The observed maximum wind speed around the mLLJ is 16 m s^{-1}, whereas the simulated maximum is 25 m s^{-1}. Although only a few wind observations are available for verification, it seems that the model simulated a stronger mLLJ at 850 hPa. Except for this bias, the model wind field is acceptable. At 700 hPa, a tongue of relatively warm, moist air is present to the south of the mesolow. Cool, dry air is located to the northwest (Fig. 14b). The θ_e and q gradients within the mesolow are rather weak. In contrast, the strong gradients of θ_e and q associated with the Mei-Yu front are located farther to the north of the mesolow. This shows that the Mei-Yu front is very shallow and slopes rapidly northward. The mesolow develops in the warm, moist air and is forced by convection.

In the upper troposphere (Fig. 14d), the synoptic-scale westerly jet is found north of 35°N. South of 35°N, the wind turns northwesterly. The mesolow is located in a diffluent region south of the synoptic jet. A mesoscale northwesterly wind maximum (24 m s^{-1}, shaded in Fig. 14c) is located ahead (east) of the mesolow. Compared with the observed wind speed of 26 m s^{-1}, the model results are quite good. This wind speed maximum is also simulated at 200 hPa (not shown). It can be regarded as a mesoscale upper-level jet (hereafter mULJ). Wind speeds behind (west of) the mesolow range from 13 to 16 m s^{-1} in both the simulation and the observations. The mULJ is located in a synoptic-scale diffluent flow over the mesolow. Upper-level divergence over the rainstorm reached 1.6×10^{-4} s^{-1} (Fig. 14d). There is a strong updraft at 700 hPa immediately to the left of the mULJ (Fig. 14e). Warm, moist air at 300 hPa is located to the east of the mesolow, indicating that the upper-level stratiform cloud extended downstream from the convection (Fig. 14f). All of these mesoscale features suggest that this mULJ is the consequence of upper-level outflow associated with the rainstorm.

f. Impact of latent heat release

In this section we examine the role of latent heat release in the formation of the mLLJ and its associated vertical circulation. An experiment with no latent heat release from either the grid-scale condensation or parameterized cumulus convection (referred to as fake dry, hereafter FDR) was carried out. In the FDR run, there was no evidence of a mesolow or mLLJ at 850 hPa (Fig. 15a). A broad southwesterly flow occupied the Jiang-Huai Basin. Wind speeds in the area where the mLLJ was simulated in the CNTL full-physics run were only about 6–8 m s^{-1}, with wind vectors nearly parallel to the height contours. Figure 15b shows the differences in 850-hPa geopotential height and wind vectors at $t = 12$ h between CNTL and FDR (CNTL − FDR). It clearly shows the impacts of latent heat release on the development of the mLLJ and the mesolow. Latent heat release in CNTL has produced a low over Jiang-Huai Basin with a depth of 74 gpm where the rainstorm was simulated. Its size is very similar to the mesolow shown in Fig. 10a. A cyclonic vortex is associated with this mesolow (Fig. 15b). It should be noted that the CNTL − FDR wind difference vectors in the mLLJ area point to the low center, which implies a strong ageostrophic wind induced by latent heating.

The vertical circulation still exists on the cross section along the line AA′ (position shown on Fig. 9) in FDR, but it is quite weak (Fig. 16b). The upward motion was only 6 cm s^{-1} as compared with 70 cm s^{-1} in the CNTL. Large differences also exist for the wind speed perpendicular to the cross section between CNTL and FDR (cf. Figs. 11a and 16a). This suggests a positive feedback process between convection and the formation of the mLLJ.

g. Sensitivity to precipitation parameterization and horizontal resolution

As discussed earlier, latent heat release is a very important forcing mechanism for the development of the mesolow. Also, most of the precipitation in the 54-km grid was produced by the resolvable-scale parameterization. This raises an important question: Was the mesolow simulated in the 54-km grid produced by unstable (and perhaps, unrealistic) feedback between the grid-scale precipitation parameterization and the Mei-Yu front, similar to the so-called runaway CISK-type instability discussed by Zhang et al. (1988). Moreover,

←

0.2 g kg^{-1}) and θ_e (dashed lines every 2 K). Simulated 1-h rainfall ($t = 23$–24 h) greater than 10 mm is stippled. Thick dashed lines in (b)–(f) are the 1430-gpm contours at 850 hPa, representing the mesolow. Observed winds are plotted in (a) and (c) with the wind speed (bold) at the base of the wind barbs.

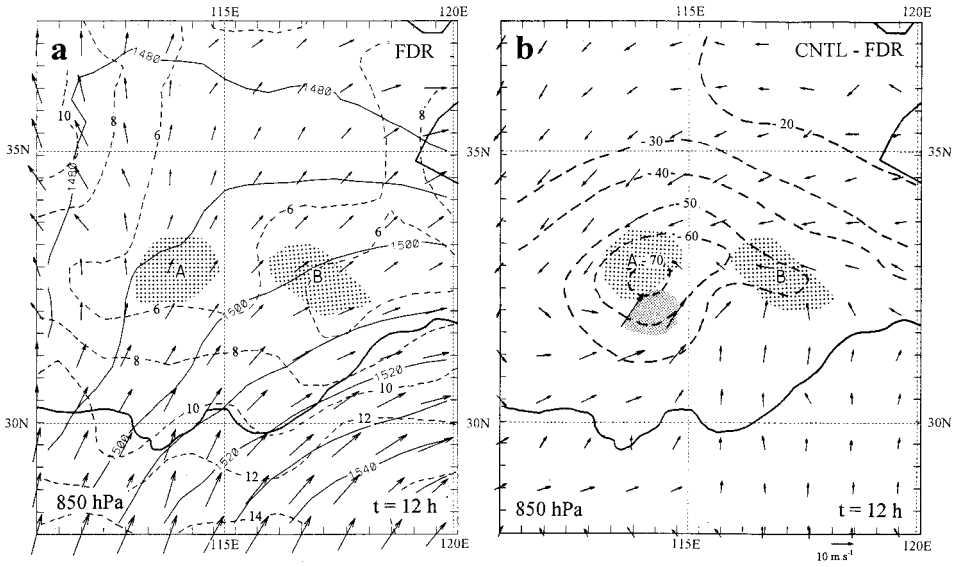

FIG. 15. (a) The 850-hPa geopotential height (thin solid lines every 10 gpm), wind vectors, and wind speeds (dashed lines every 2 m s^{-1}) at $t = 12$ h simulated in experiment FDR. (b) Difference of 12-h simulated 850-hPa height (dashed lines every 10 in gpm) and wind vectors for the CNTL minus FDR at $t = 12$ h. Rainstorms (stippled) and mLLJ (shaded) simulated in the CNTL are shown for reference.

how was the result sensitive to different choices of subgrid-scale convective parameterization and grid size?

Molinari and Dudek (1992) showed that absolutely unstable and unrealistic soundings (see Fig. 1 of their paper) can be produced by a mesoscale model in the simulation of a mesoscale convective system with only explicit (resolvable scale) precipitation parameterization (without subgrid-scale convective parameterization). The basic problem is that the resolvable-scale precipitation is ineffective in stabilizing a convective environment with large convective available potential energy (CAPE; because the vertical motion is much too slow in a mesoscale model as compared with that of a cloud model). Strong latent heat release in the lower tropo-

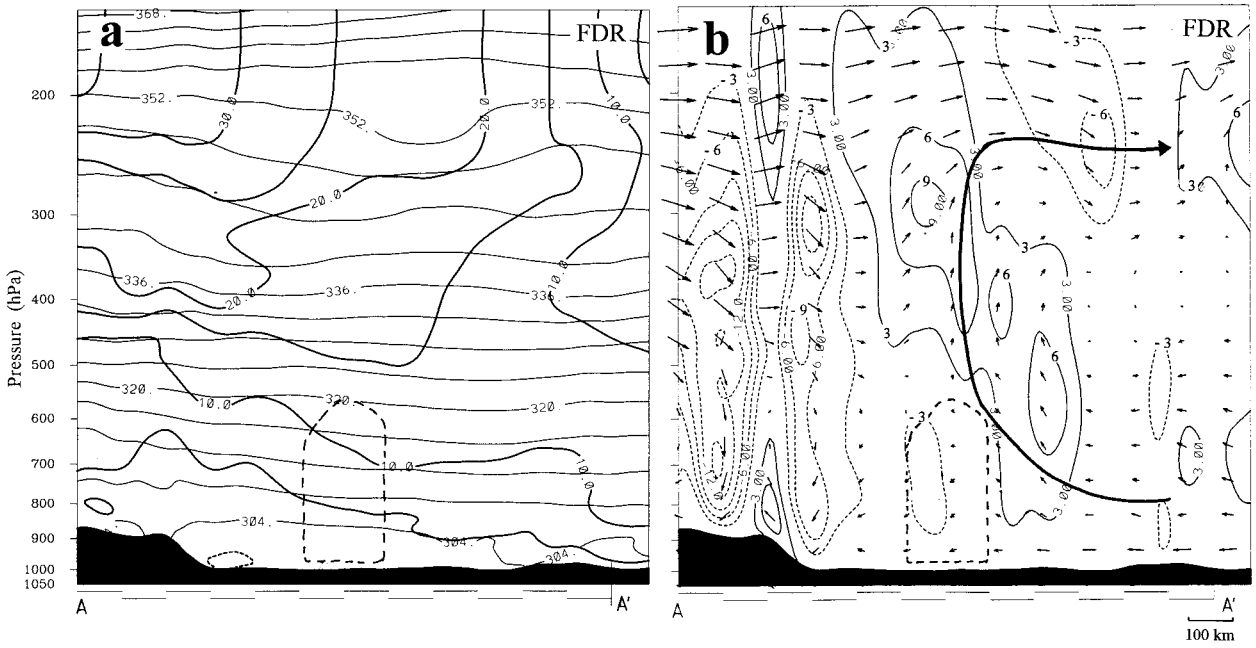

FIG. 16. Vertical cross sections along line AA′ in Fig. 8 in the FDR run. (a) Potential temperature (q, thin lines every 4 K) and wind speed normal to the cross section (V_n, thick lines every 5 m s^{-1}). (b) In-plane vertical circulation and vertical velocity (every 3 cm s^{-1}). The dashed lines indicate the rainstorm in the CNTL.

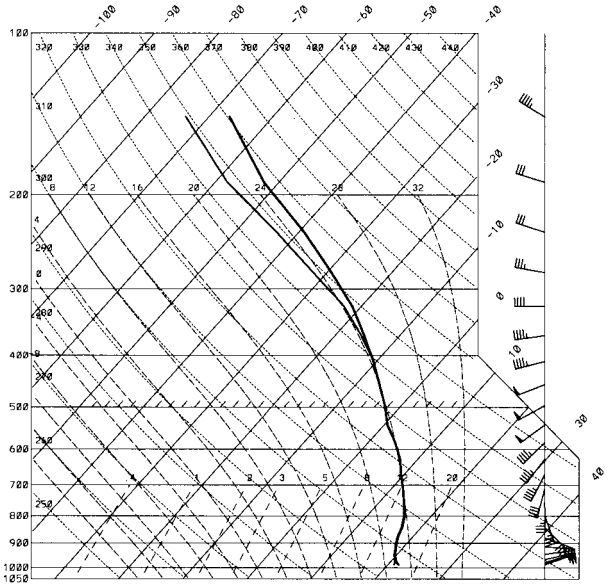

FIG. 17. Simulated sounding plotted in skew *T* diagram from CNTL at $t = 12$ h (1200 UTC 12 June). The location of the sounding is shown in Fig. 9.

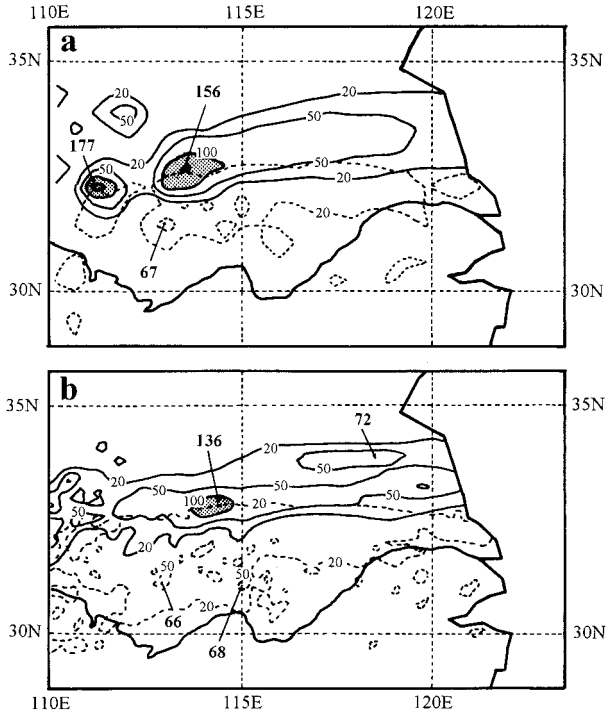

FIG. 18. Simulated 24-h rainfall produced in experiments using the Kain–Fritsch cumulus scheme (dashed) and explicit scheme (solid) from (a) the 54-km experiment (KF54) and (b) the 18-km experiment (KF18). Areas with rainfall exceeding 100 mm are shaded.

sphere induces strong moisture convergence, which in turn stimulates additional convection, establishing an unstable feedback. As a result, fictitious low pressure centers can develop quickly in a mesoscale model with only the resolvable-scale precipitation parameterization (Zhang et al. 1988). In a large CAPE environment, a good convective parameterization would consume a good portion of the convective instability, and transport heat and moisture from the lower troposphere to the upper troposphere, and allow the mesoscale stratiform precipitation to develop naturally (Kuo et al. 1997).

The dominance of resolvable-scale precipitation in the 54-km CNTL simulation with the Grell scheme could be a result of the convective environment of the Mei-Yu (high moisture and low CAPE), or a reflection of the deficiency of the subgrid-scale convective parameterization. To assess the realism of the CNTL simulation, we plotted a model sounding in the middle of rainstorm A (location marked as ''×'' in Fig. 9) at the time when it was producing heavy precipitation (33 mm h^{-1}) in Fig. 17. The temperature profile closely follows the moist-adiabatic lapse rate from 800 through 400 hPa. It is saturated from the surface to 400 hPa. This is a near-neutral sounding with little or no convective instability. Apparently, the model was able to consume the convective instability effectively through resolvable-scale precipitation parameterization. Below 800 hPa, the sounding shows a cold and saturated boundary layer, which is possibly a result of downdrafts produced by the resolvable-scale precipitation parameterization. This is a realistic looking sounding, unlike the one shown in Molinari and Dudek (1992).

To assess the sensitivity of the model results to the choice of different convective parameterizations, we repeated the simulation with the Kain–Fritsch (1993) scheme for subgrid-scale convection. The results are shown in Fig. 1d. The peak rainfall amounts are 196 and 172 mm, respectively, for the two heavy rainfall cells, which are weaker than the corresponding values of 262 and 310 mm in CNTL (Fig. 1b). The partitioning of precipitation into resolvable and subgrid-scale components are shown in Fig. 18a. A comparison between Figs. 1c and 18a indicate similar precipitation characteristics between these two simulations: 1) The location of the rainfall belt is nearly identical, 2) the heavy rainfall cells are predicated at the same loci, 3) resolvable-scale precipitation dominates the precipitation process, and 4) convective precipitation is located to the south of resolvable-scale precipitation. Although different convective schemes were used, the precipitation characteristics are highly similar to one another.

Figure 19a shows the 850-hPa height field and wind vectors for the 54-km Kain–Fritsch experiment at $t = 12$ h. Although a closed low has not yet formed at this time, the height field clearly indicates a deepening trough. Indeed, a closed low formed 3 h later. The slightly slower development is related to the weaker precipitation simulated by the KF54 experiment using the Kain–Fritsch scheme. However, the track and life cycle of the rainstorms and the mesolow evolution in KF54 are very similar to the CNTL experiment.

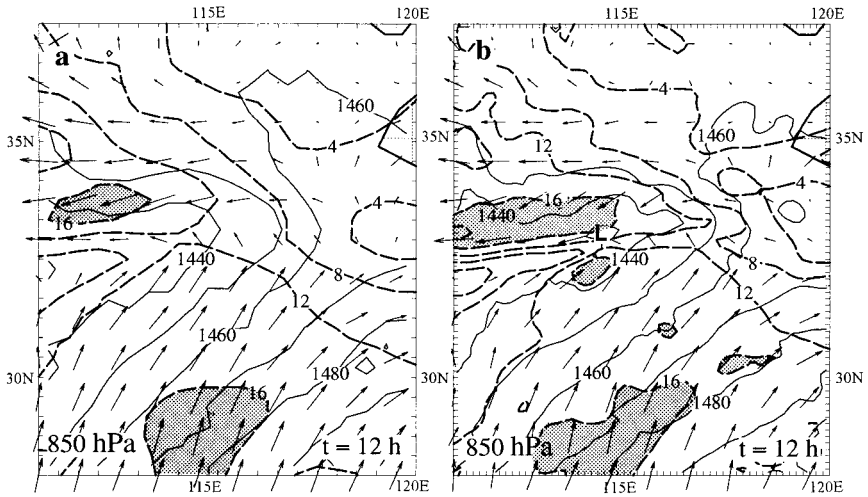

FIG. 19. Simulated 850-mb geopotential height (thin solid lines every 10 gpm), wind speed (thick dashed lines every 4 m s^{-1}), and wind vectors from the Kain–Fritsch experiments at (a) 54 km and (b) 18 km. Areas with wind speed exceeding 16 m s^{-1} are shaded.

To assess the sensitivity of the model simulation to grid resolution, we repeated the Kain–Fritsch experiment with a grid size of 18 km. Interestingly, the precipitation characteristics are not altered drastically with increased grid resolution (Fig. 18), although the details of the rainfall distribution are different. Still, the precipitation is dominated by the resolvable-scale rainfall, and the convective precipitation takes place on the southern part of the rainfall belt. The 18-km Kain–Fritsch simulated a closed mesolow at $t = 12$ h (Fig. 19b), with its intensity and position closely resembling that of CNTL.

The results from these two additional experiments using the Kain–Fritsch scheme at both 54- and 18-km grid size provide strong support to the validity and realism of the CNTL experiment. A question can be asked: Why should the resolvable-scale rainfall dominate the precipitation process along a Mei-Yu front? How does it differ from the summertime or springtime convective systems in the United States? The answer may lie in the differences in convective environments. The environment along (or immediately to the south of) the Mei-Yu front is highly moist and is characterized with low CAPE. In contrast, a typical springtime central U.S. convective environment is usually much drier and possesses a much larger CAPE. In such an environment, a subgrid-scale convective parameterization scheme should be activated to produce a large fraction of the model precipitation. However, in a highly saturated Mei-Yu environment, most of the precipitation may be produced by steady large-scale vertical motion. Subgrid-scale convection does not contribute as much toward the total precipitation. Because the environment is very moist, the simulation of Mei-Yu precipitation may be less sensitive to convective parameterization, as compared to that of a much drier and high-CAPE environment.

6. Summary and discussion

On 12–13 June 1991, a series of mesoscale convective systems developed along an east–west-oriented Mei-Yu front through eastern China. The first of these, denoted system D, embedded within the SW vortex. This convective system, D, moved eastward into a convectively unstable region south of the Mei-Yu front. As system D started to weaken, a new convective system (A′) formed about 400 km to the east of D. System A′ moved eastward and reached its maturity in about 8 h. At that time, another system, B′, formed about 300 km to the east of A′. While A′ began to decay, B′ continued to move eastward and grew rapidly. Approximately 8 h later, B′ reached maturity, while yet another system, C′, formed to the east of B′. The sequential development and eastward propagation of these mesoscale convective systems (particularly A′ and B′) brought heavy precipitation to the Jiang-Huai Basin of eastern China, where a maximum 24-h accumulation of 234 mm was observed.

As the size of these mesoscale convective systems at their mature stage was on the order of 500 km × 500 km, their internal structures could not be adequately resolved by routine upper-air observations. Furthermore, although system A′ went through its life cycle over mainland China (i.e., over a region covered by surface and upper-air observing networks), the other systems did not. System B′, for example, was initiated over eastern China, but soon moved offshore. It was found that as system A′ matured, a shallow, meso-α-scale low formed along the Mei-Yu front and embedded

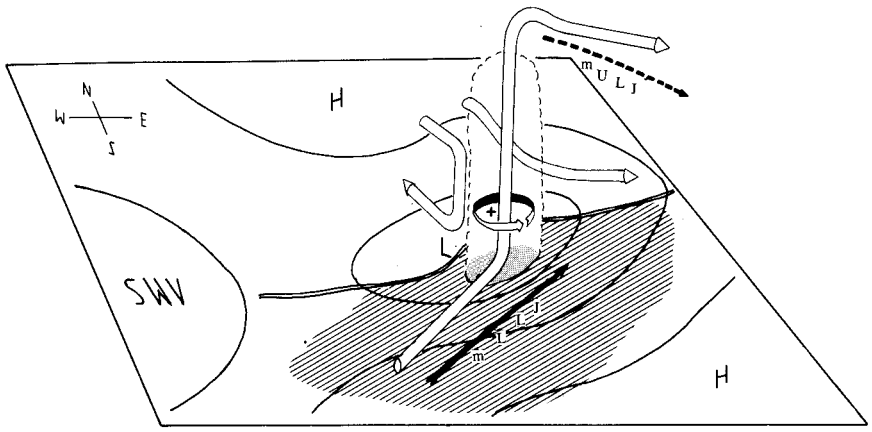

FIG. 20. Schematic diagram of the meso-α-scale low and associated rainstorm. The center of the mesolow is indicated by ''L.'' ''SWV'' is the SW vortex. The cylindrical arrows show the trajectories of the low-level warm air and the midtropospheric cool air, the thin solid lines are 850-hPa height contours, the cloud outline is the rainstorm area, the circular arrows show the relative vorticity, the thick solid and dashed arrows are the LLJ and ULJ at 850 and 300 hPa, respectively, the double line indicates the surface Mei-Yu front, and the stippled area indicates the high θ_e and convective unstable area.

the convective system in its center. Whether systems B′ and C′ were associated with such mesolows is not known, since these systems reached their mature stage over the ocean where upper-air observations are lacking.

We performed a control simulation of this heavy rainfall event using the MM5 at a horizontal resolution of 54 km. The model's moist process package consisted of a mixed-phase scheme for resolvable-scale precipitation and the Grell scheme for subgrid-scale convection. The model was initialized with standard synoptic upper-air and surface observations and was integrated for 24 h. Despite the relatively coarse horizontal resolution, the model simulated many of the features observed in this case, including 1) the sequential development of the rainstorms at an interval of 300–400 km, 2) the 24-h accumulated precipitation exceeding 150 mm over the Jiang-Huai Basin, 3) the development of mesoscale low-level jets (mLLJ) to the south of the rainstorms, and 4) the formation of a mesolow associated with one of the rainstorms. The successful simulation of this heavy rainfall event allows examinations of the detailed mesoscale structure associated with the Mei-Yu frontal rainstorms, their governing dynamics, and their interaction with the Mei-Yu front.

After careful analysis of the model simulation a conceptual model for a Mei-Yu rainstorm emerges and is schematized in Fig. 20. As a convective system initiated in the southwest vortex moves eastward into a convectively unstable region south of the Mei-Yu front, the system excites the development of a series of rainstorms, with each storm forming 300–400 km to the east of the preceding storm. Each rainstorm has a lifetime of about 18–24 h. Strong latent heat release associated with a rainstorm (with maximum hourly rainfall rates exceeding 50 mm) produces strong vertical motion, low-level convergence, and upper-level divergence. The strong low-level convergence, interacting with both the low-level horizontal wind shear associated with the Mei-Yu front and the background earth rotation, leads to rapid vorticity spinup. At the mature stage of a rainstorm, the relative vorticity and the potential vorticity reach fairly large values (e.g., $\sim 5 \times 10^{-4}$ s^{-1} and 3 PVU, respectively), and a meso-α-scale low develops. As a rainstorm develops, a southerly mLLJ forms to its south and the low-level easterly flow to the north of the front is enhanced. The southerly mLLJ is particularly important in bringing warm, moist air to support the development of the rainstorm, and the jet remains highly ageostrophic even at the storm's mature stage. At upper levels, it is found that the outflow associated with a rainstorm produces a mesoscale upper-level jet immediately downstream of the system. The southerly mLLJ, the strong rising motion associated with the rainstorm, and the upper-level outflow greatly enhance a synoptic-scale vertical circulation associated with the Mei-Yu front.

An experiment without condensational heating showed that latent heat release was crucial for the development of the rainstorm, the mLLJ, the mesolow, the mesoscale upper-level outflow, and the rapid spinup of vorticity. The experiment also showed that the Mei-Yu front was weakened considerably in the absence of the latent heating associated with the rainstorm. These results suggest that there is strong interaction and positive feedback between convective rainstorms in the Mei-Yu frontal region and the Mei-Yu front itself. In short, the front provides a favorable environment for such rainstorms to develop, while the rainstorms intensify the front. A similar positive feedback also exists between a southerly mLLJ and a rainstorm.

These results suggest that the rainstorms observed

along the Mei-Yu front can be viewed as diabatically driven mesoscale circulation systems in a potentially unstable environment with weak baroclinicity. The Mei-Yu front (with convectively unstable air to its south, horizontal wind shear, and low-level baroclinicity) provides a favorable environment for these rainstorms to develop. After the storm is initiated, the release of latent heat induces the mLLJ, which enhances storm development, which, in turn, intensifies the Mei-Yu front.

Analysis of the full-physics control experiment shows that the precipitation was dominated by the resolvable-scale component. Two additional experiments that employed the Kain–Fritsch convective parameterization scheme with grid sizes of 54 and 18 km produced similar precipitation characteristics. The dominance of grid-scale precipitation is attributed to the high relative humidity and low CAPE in the environment of a Mei-Yu front.

The results derived from this numerical study need to be generalized with additional case studies. The scarcity of mesoscale observations hinders the understanding of the mesoscale features associated with the Mei-Yu front, and verification of the simulated mesoscale features associated with the rainstorms. It is encouraging that the results presented in this study showed that the MM5, even at a horizontal resolution comparable to that of most operational models, is capable of simulating mesoscale convective systems observed along the Mei-Yu front.

A number of important questions remain to be answered. These include the following: (i) Why do new rainstorms develop sequentially at intervals of 300–400 km to the east of preceding storms? (ii) What determines the scale of this 300–400-km wavelength? (iii) Do rainstorms always induce mesolows (or mesoscale cyclones along the Mei-Yu front)? (iv) How realistic are the simulated mesoscale LLJs? Special observations from mesoscale field programs during the Mei-Yu season and high-resolution model simulations of observed events are needed to address these questions.

Acknowledgments. We are grateful to Drs. Richard Reed, Lance Bosart, Howard Bluestein, Jim Bresch, Scott Braun, Jimy Dudhia, Chaing Chen, Shang-Wu Li, Jordan Powers, and two anonymous reviewers for their valuable comments that helped improve this paper. Shou-Jun Chen would like to express his appreciation to Dr. Robert Gall, director of Mesoscale and Microscale Meteorology Division, for supporting his visit to NCAR. This work is partially supported by NASA/Goddard under Order S-41381-F, and partially supported by the Chinese Natural Science Foundation under Grant 49335060.

REFERENCES

Anthes, R. A., Y.-H. Kuo, S. G. Benjamin, and Y.-F. Li, 1982: The evolution of the mesoscale environment of severe local storms: Preliminary modeling results. *Mon. Wea. Rev.,* **110,** 1187–1213.

Chen, C., W.-K. Tao, P.-L. Lin, G. S. Lai, S.-F. Tseng, and T.-C. Chen Wang, 1998: The intensification of the low-level jet during the development of mesoscale convective systems on a Mei-Yu front. *Mon. Wea. Rev.,* **126,** 349–371.

Chen, G. T.-J., 1983: Observational aspects of Mei-Yu phenomena in subtropical China. *J. Meteor. Soc. Japan,* **61,** 306–312.

——, and C.-C. Yu, 1988: Study of low-level jet and extremely heavy rainfall over northern Taiwan in the Mei-Yu season. *Mon. Wea. Rev.,* **116,** 884–891.

Chen, Q.-S., 1982: The instability of the gravity–inertia wave and its relation to low-level jet and heavy rainfall. *J. Meteor. Soc. Japan,* **60,** 1041–1057.

Chen, Y.-L., X.-A. Chen, and Y.-X. Gang, 1994: A diagnostic study of the low-level jet during TAMEX IOP5. *Mon. Wea. Rev.,* **122,** 2257–2284.

——, ——, S. Chen, and Y.-H. Kuo, 1997: A numerical study of the low-level jet during TAMEX IOP5. *Mon. Wea. Rev.,* **125,** 2583–2604.

Chou, L. C., C.-P. Chang, and R. T. Williams, 1990: A numerical simulation of the Mei-Yu front and the associated low level jet. *Mon. Wea. Rev.,* **118,** 1408–1428.

Ding, Y.-H., 1992: Summer monsoon rainfalls in China. *J. Meteor. Soc. Japan,* **70,** 337–396.

Dong, L., 1991: The weather in June 1991 (in Chinese). *Meteor. Mon.,* **17,** 58–61.

Dudhia, J., 1993: A nonhydrostatic version of the Penn State–NCAR mesoscale model: Validation tests and simulation of an Atlantic cyclone and the cold front. *Mon. Wea. Rev.,* **121,** 1493–1513.

Fang, Z.-Y., 1985: Preliminary study of medium-scale cloud cluster over Changjiang basin in summer. *Adv. Atmos. Sci.,* **2,** 334–340.

Feng, Z.-X., N. Zheng, and J.-X. Yang, 1995: Mesoscale analysis of a heavy precipitation event over Jiang-Huai Basin (in Chinese). *Studies on Heavy Rainfall over Jiang-Huai Basin in 1991,* Y.-H. Ding, Ed., Meteor. Press, 120–124.

Grell, G. A., J. Dudhia, and D. R. Stauffer, 1994: A description of the fifth-generation Penn State/NCAR mesoscale model (MM5). NCAR Tech. Note NCAR/TN-398+STR, 138 pp.

Hibbard, W., and D. Santek, 1990: The VIS-5D system for easy interactive visualization. *Proc. Visualization '90,* San Francisco, CA, IEEE, 28–35.

Holton, J. R., 1990: *An Introduction to Dynamic Meteorology.* 3d ed. Academic Press, 511 pp.

Kain, J. S., and J. M. Fritsch, 1993: Convective parameterization for mesoscale models: The Kain–Fritsch scheme. *The Representation of Cumulus Convection in Numerical Models, Meteor. Monogr.,* No. 46, Amer. Meteor. Soc., 165–170.

Kato, K., 1985: On the abrupt change in the structure of the Baiu front over the China continent in late May of 1979. *J. Meteor. Soc. Japan,* **63,** 20–36.

Kuo, Y.-H., and G. T.-J. Chen, 1990: The Taiwan Area Mesoscale Experiment (TAMEX): An overview. *Bull. Amer. Meteor. Soc.,* **71,** 488–503.

——, L. Cheng, and R. A. Anthes, 1986: Mesoscale analyses of the Sichuan flood catastrophe, 11–15 July 1991. *Mon. Wea. Rev.,* **114,** 1984–2003.

——, J. F. Bresch, M.-D. Cheng, J. Kain, D. B. Parsons, W.-K. Tao, and D.-L. Zhang, 1997: Summary of a mini-workshop on cumulus parameterization for mesoscale models. *Bull. Amer. Meteor. Soc.,* **78,** 475–491.

Li, Y.-L., S.-Y. Tao, and C.-X. Du, 1993: An analysis of the meso-convective cloud clusters in Mei-Yu front (in Chinese). *Quart. J. Appl. Meteor.,* **4,** 278–285.

Ma, K.-Y., and L. F. Bosart, 1987: A synoptic overview of a heavy rain event in southern China. *Wea. Forecasting,* **2,** 89–112.

Molinari, J. M., and M. Dudek, 1992: Parameterization of convective precipitation in mesoscale numerical models: A critical review. *Mon. Wea. Rev.,* **120,** 326–344.

Nagata, M., and Y. Ogura, 1991: A modeling case study of interaction

between heavy precipitation and a low-level jet over Japan in the Baiu season. *Mon. Wea. Rev.*, **119,** 1309–1336.

Ninomiya, K., and T. Murakami, 1987: The early summer rainy season (Baiu) over Japan. *Monsoon Meteorology*, C. P. Chang and T. Krishnamurti, Eds., Oxford University Press, 93–121.

——, H. Koga, Y. Yamagish, and Y. Tatsumi, 1984: Prediction experiment of extremely heavy rainstorm by fine mesh primitive equation model. *J. Meteor. Soc. Japan*, **62,** 273–295.

Ogura, Y., H.-M. Juang, K.-S. Zhang, and S.-T. Soong, 1982: Possible triggering mechanisms for severe storms in SESAME-AVE IV (9–10 May 1979). *Bull. Amer. Meteor. Soc.*, **63,** 503–515.

Reisner, J., R. T. Bruintjes, and R. J. Rasmussen, 1998: Explicit forecasting of supercooled water in winter storms using the MM5 mesoscale model. *Quart. J. Roy. Meteor. Soc.*, **124B,** 1071–1107.

Xiang, X., M. Lan, and D. Wang, 1993: The mesoscale analysis of the Mei-Yu front cloud system in 1991 (in Chinese). *Quart. J. Appl. Meteor.*, **4,** 288–292.

Zhang, D., and R. A. Anthes, 1982: A high-resolution model of the planetary boundary layer—Sensitivity tests and comparisons with SESAME-79 data. *J. Appl. Meteor.*, **21,** 1594–1609.

——, E.-Y. Hsie, and M. W. Moncrieff, 1988: A comparison of explicit and implicit predictions of convective and stratiform precipitating weather systems with a meso-β scale numerical model. *Quart. J. Roy. Meteor. Soc.*, **114,** 31–60.

——, K. Gao, and D. B. Parsons, 1989: Numerical simulation of an intense squall line during 10–11 June 1985 PRE-STORM. Part I: Model verification. *Mon. Wea Rev.*, **117,** 960–994.

Zhu, Q.-G., J.-R. Lin, and S.-W. Shou, 1981: *Principles and Methods in Synoptic Meteorology* (in Chinese). Beijing Meteorological Press, 535 pp.